Historical Earthquake Scenarios for the Middle Strand of the North Anatolian Fault Deduced from Archeo-Damage Inventory and Building Deformation Modeling

Yacine Benjelloun, Julia Sigoyer (de), Hélène Dessales, Laurent Baillet, Philippe Gueguen, Mustafa Sahin

Seismological Research Letters

Historical earthquake scenarios for the middle strand of the North Anatolian Fault deduced from archeo-damage inventory and building deformation modeling

--Manuscript Draft--

Manuscript Number:	SRL-D-20-00278R2
Full Title:	Historical earthquake scenarios for the middle strand of the North Anatolian Fault deduced from archeo-damage inventory and building deformation modeling
Article Type:	Historical Seismologist
Corresponding Author:	Yacine Benjelloun, Ph.D. Institut De Physique Du Globe De Paris Paris, Ile-de-France FRANCE
Corresponding Author Secondary Information:	
Corresponding Author's Institution:	Institut De Physique Du Globe De Paris
Corresponding Author's Secondary Institution:	
First Author:	Yacine Benjelloun, Ph.D.
First Author Secondary Information:	
Order of Authors:	Yacine Benjelloun, Ph.D.
	Julia de Sigoyer
	Hélène Dessales
	Laurent Baillet
	Philippe Guéguen
	Mustafa Sahin
Order of Authors Secondary Information:	
Manuscript Region of Origin:	
Suggested Reviewers:	Shmuel Marco, Ph.D. Professor, Tel Aviv University shmulikm@tauex.tau.ac.il Significant experience in archeoseismology
	Miguel Angel Rodriguez-Pascua, Ph.D. Researcher, Instituto Geológico y Minero de España ma.rodriguez@igme.es Significant experience in archeoseismology
	Manuel Sintubin, Ph.D. Professor, KU Leuven manuel.sintubin@kuleuven.be Significant experience in earthquake archeology
	Chris Gerrard, Ph.D. Professor, Durham University c.m.gerrard@durham.ac.uk Manager of several projects studying seismic events in the Middle Ages.

Historical earthquake scenarios for the middle strand of the North Anatolian Fault deduced from archeo-damage inventory and building deformation modeling

Yacine Benjelloun[1], Julia de Sigoyer[2], Hélène Dessales[3], Laurent Baillet[2], Philippe Guéguen[2], Mustafa Sahin[4]

1 : Université de Paris, Institut de physique du globe de Paris, CNRS, F-75005 Paris, France

2 : Univ. Grenoble Alpes, Univ. Savoie Mont Blanc, CNRS, IFSTTAR, IRD, ISTerre, 38000 Grenoble, France

3 : ENS, UMR 8546, Laboratoire AOROC-ENS, 75230 Paris, France

4 : Fen-Edebiyat Fakültesi, Arkeologi Bölümü, Uludag Üniversitesi, Bursa, Turkey

Corresponding author :

Yacine Benjelloun

Institut de Physique du Globe - UMR7154

1, rue Jussieu

75238 Paris cedex 05, France

+33 (0)6 80 21 52 44

benjelloun@ipgp.fr

Abstract

The city of Iznik (ancient Nicaea), located on the middle strand of the North Anatolian fault zone (MNAF), presents outstanding archeological monuments preserved from the Roman and Ottoman periods (1^{st}-15^{th} c. AD), bearing deformations which can be linked to past seismic shaking. In order to constrain the date and intensity of these historical earthquakes, a systematic survey of Earthquake Archeological Effects (EAE) is carried out on the city's damaged buildings. Each of the 235 EAE found is given a quality ranking and the corresponding damage is classified according to the EMS98 scale. We show that the walls oriented N-S were preferentially damaged, and that most deformations are perpendicular to the walls' axes. The date of postseismic repairs is constrained with available archeological data and new ^{14}C dating of mortar charcoals. Three damage episodes are evidenced: (1) between the 6^{th} and late 8^{th} centuries, (2) between the 9^{th} and late 11^{th} centuries AD, (3) after the late 14^{th} century AD. The repartition of damage as a function of building vulnerability points toward a global intensity VIII on the EMS98 scale. The 3D modeling of a deformed Roman obelisk shows that only earthquakes rupturing the MNAF can account for this deformation. Their magnitude can be bracketed between Mw 6 and 7. Our archeoseismological study complements the historical seismicity catalogue and confirms paleoseismological data, suggesting several destructive earthquakes along the MNAF since the first century AD. We suggest the fault might still have accumulated enough stress to generate a Mw 7+ rupture.

INTRODUCTION

Documenting the calendar of past earthquakes in tectonically active regions is an important step to determine their seismic hazard (Guidoboni and Stucchi, 1993; Bilham et al., 2001). In certain contexts, the knowledge of Holocene earthquakes is the only way to estimate the magnitude range expectable in a given area and the recurrence times between big earthquakes. Paleoseismological trenching allows one to identify the last ruptures in the stratigraphy at a given point of the fault (McCalpin, 2009).

Historical seismology has been developed to build earthquake catalogues using written descriptions of seismic events (Ambraseys, 2000, 2002). Whereas palaoseismology is primarily concerned with the source of earthquakes, historical seismology interprets the observable consequences in the form of intensities felt at given locations.

Evidence of coseismic deformation found in the stratigraphy of archeological survey sites and on ancient buildings has been increasingly described and used to complement earthquake catalogues and, in some cases, quantitatively constrain earthquakes thanks to numerical modeling (Korzhenkov and Mazor, 1999; Mazor and Korzhenkov, 2001; Hinzen, 2005). Although the interpretation of archeological evidence is delicate because possible traces of earthquakes are rarely unambiguous, this “archeoseismological” approach allows one to document past earthquakes in regions without written archives, which extends the time scale of the catalogue (Karcz and Kafri, 1978). The archeological record may also preserve smaller events that are poorly preserved in classical trenches (Rapp, 1986).

In this study, we apply this archeoseimological approach to the city of Iznik (ancient Nicaea), located 3 km north of the active fault segments of the middle strand of the North Anatolian fault (MNAF, Fig. 1). Since the beginning of the instrumental period, this fault strand has been characterized by a very low seismicity and deformation rate (Özener et al., 2013; Öztürk et al., 2009). However, various datasets documenting the pre-instrumental seismic activity strongly contrast with this modern quiescence. The historical record of ancient earthquakes having affected Iznik (Fig. 2) contains no less than ten destructive earthquakes during the last two millennia (Ambraseys and Finkel, 1991; Ambraseys and Jackson, 1998, 2000; Ambraseys, 2000, 2002, 2009; Guidoboni et al., 1994). The compilation of the paleoseismic trench data along the MNAF suggests the occurrence of at least four Mw 6+ earthquakes during the last two millennia (Barka, 1992, 1993; Dogan, 2010; Ikeda, 1988; Ikeda et al., 1989; Özalp et al., 2013; Yoshioka & Kusçu, 1994). Moreover, the region presents several archeological clues suggesting past earthquake occurrence, such as the submerged basilica recently discovered in Iznik

Lake (Sahin & Fairchild, 2018), and the numerous traces of deformation and reconstruction on the city's ancient buildings (Benjelloun et al., 2018). Despite this evidence of past earthquakes, more precise data are needed to perform a reliable assessment of seismic hazard for the Iznik region.

The goal of this study is to use the ancient buildings in Iznik and its surroundings as records of past seismicity. The compilation of many traces of potential earthquake damage provides a complementary dataset to historical seismology and paleoseismology in order to discuss the level of seismic activity of the MNAF during the last 2000 years. The dating of several independent buildings affected by earthquake shaking, and their repairs, allows us to complement the earthquake catalogue. The modeling of archeoseismic damage helps to discuss the epicenter location and strength of the earthquakes responsible for the damage observable today in the city.

TECTONIC CONTEXT OF THE STUDY: THE MNAF AND IZNIK'S SEISMIC LANDSCAPE

The study area includes the city of Iznik and its close surroundings, in the southeast of the Marmara Sea (Fig. 1 and 3a). It is located on the middle branch of the North Anatolian fault. The North Anatolian Fault zone (NAFZ) is a major tectonic boundary accommodating the relative motion between the Eurasian and Anatolian plates. It is a 1000-km long, right-lateral strike-slip fault crossing the northern part of Turkey (Sengör, 1979). This fault zone is associated with a significant seismic hazard and with several destructive earthquakes since the beginning of the Common Era (Fig. 2).

In its western termination, the NAFZ is divided into three strands (Fig. 1). The northern strand (NNAF) continues along the strike of the main fault zone and crosses the northern part of the Marmara Sea from Izmit Gulf to Gelibolu Peninsula. This strand was especially involved in the last seismic crisis that occurred as a succession of ruptures migrating westwards, from Erzincan in 1939 to Izmit in 1999 (Stein et al., 1997). The middle strand (MNAF) separates from the NNAF in the Akyazi district, borders on the south two successive basins known as the Geyve-Pamukova Basin and Iznik Lake, reaches the Marmara

Sea through Gemlik Gulf and borders the southern shore of the Marmara Sea (Fig. 3a). With a relative horizontal motion estimated around 5 mm/year with GPS (Ergintav et al., 2014), the MNAF shows a deformation rate five times smaller than the NNAF (~20-25 mm/year) (Reilinger et al., 2006). The southern strand (SNAF) separates from the MNAF near Iznik and continues southwestwards to Ulubat and Manyas Lakes (Fig. 1).

In addition to the MNAF, smaller structures around Iznik Lake show morphological evidence of recent activity. North of the lake, two oblique fault zones, the NW-SE striking Orhangazi fault (Fig. 3a) and the ENE-WSW striking Boyalica fault, separate the basement rocks of the Armutlu block and the Quaternary alluvia of the lacustrine plain (Öztürk et al., 2009). A small normal fault zone, the Elbeyli fault, was described east of Iznik, forming a 7 km long scarp at the foot of a marble and schist massif, cross-cutting in the south the eastern section of the Iznik aqueduct (Benjelloun et al., 2018).

The natural environment of Iznik presents cumulative expression of Holocene and historical coseismic effects, such as faceted scarps (Fig. 3b), meter scale recent scarplets evidenced on land (Ikeda et al., 1989) and in the bathymetry of Iznik Lake (Gastineau et al., 2020 PREPRINT), laterally offset geomorphic markers (Ikeda, 1988; Sipahioglu and Matsuda, 1986; Yoshioka and Kusçu, 1994), and transtensional basins (Dogan et al., 2015). This leads geologists to qualify the city's geological environment as a "seismic landscape", as defined by Michetti et al. (2005). The most prominent earthquake source for the Iznik region is the MNAF, which represents a 140 km long dextral fault zone between Akyazi district and Gemlik. A rupture propagating along this whole section would correspond to a Mw 7.6±0.3 earthquake (Wells and Coppersmith, 1994).

ARCHEOSEISMOLOGICAL DATA COLLECTION

The main principle of an archeoseismological investigation is to look for traces of past earthquake deformation in archeological features, which are commonly called Earthquake Archeological Effects

(EAE; Rodriguez-Pascua et al., 2011). These EAE can be located on-fault, when an archeological structure is crossed and deformed by an active fault. However, the most numerous archeoseismic observations are located off-fault and concern buildings which have been deformed because of coseismic ground motion. Finally, we include in EAE the evidence for postseismic reconstructions which serve to repair a building damaged during an earthquake and/or to make it more resistant to future earthquakes.

In Iznik and its surroundings, systematic archeoseismic observations were made on the visible ancient remains (Fig. 4 and 5; for the complete list see Tables S2 and S3 in the electronic supplement). We focused our observations on the critical buildings of the city, such as the aqueduct and the defensive walls, which were especially important for its viability and were likely repaired as soon as damaged. The types of inventoried EAE in Iznik include: wall facing collapses, wall warping, wall tilting, cracks, unusual wall offsets, masonry dislocations, block rotations, block corner expulsions, block shifting, damaged arches, dropped keystones, arch collapses, column tilting, expulsion of building corner, and deformed pavement (Kazmér, 2014; Rodriguez-Pascua et al., 2011). To this dataset we also added suspected traces of post-seismic repairs and reconstructions: presumed “seismoresistant” techniques, buttresses, filling of damaged masonry with new materials, partial reconstruction of a damaged building, filling of windows and crenellations, massive reuse of materials taken from older buildings.

Each individual observation was given an identification code. This code is composed of a prefix related to the nature or category of building (AQ for the aqueduct, W for the defensive walls, C for the *intra muros* buildings and O for the obelisk) and a number. For suspected post-seismic repairs and constructions, an R is added at the beginning of the ID. The observations were geolocalized and the nature of the associated deformation or reconstruction was reported. Whenever possible, we measured the azimuth of the damaged wall, and the amount of displacement (lateral shift, vertical drop, angle of tilting). For oriented deformations, we also measured the azimuth (i.e. axis of the deformation, between 0 and 180°) and strike (i.e. direction between 0 and 360°) of the deformation.

In the following sections, when referring to the defensive walls, we use the naming conventions of Schneider and Karnapp (1938) and Foss and Winfield (1986). Each tower is numbered from T1 to T114 starting from Yenisehir Gate in the south and progressing anti-clockwise (Fig. 6b). Each wall section is numbered according to the adjacent towers (e.g. W1/2 for the wall section between T1 and T2).

For each EAE, we used a quality factor between 1 and 3, reflecting the probability of seismic origin of the deformation versus other causes (e. g. anthropic damage, natural decay, soil instability). We assign a quality 1 (good) when the seismic origin is the most probable scenario for the EAE and other processes can be discarded. When the EAE can be associated with one non-seismic process in addition to the seismic scenario, we assign a quality 2 (average). When the seismic origin is dubious because many other processes may be invoked to explain the observed deformation, we assign a quality 3 (bad). The cases of damage were also classified on a damage scale ranging from 1 to 5 (1 corresponding to very slight damage and 5 to complete destruction) and the buildings investigated were classified on a vulnerability scale (Grünthal & Levret, 2001).

On several EAE, construction material (brick, mortar) was sampled in the original structures and the repairs to constrain the date of damage. Carbonate concretion deposits on the aqueduct formed during potentially coseismic massive leakage episodes were also sampled to date the associated damage.

DESCRIPTION OF THE BUILDINGS STUDIED

The Roman obelisk at Elbeyli

6 km north of Iznik, near the village of Elbeyli, stands a Roman obelisk built during the 1st century AD (Fig. 6a and 7). The column is made of five triangular prismatic stones lying on a rectangular pedestal

(Fig. 7). Small offsets between the triangular stones suggest translation and rotation motions probably during seismic shaking (Fig. 7b,c).

The aqueduct of Iznik

The remains of two aqueducts are visible in the east of Iznik. One was discovered in 2019 outside of the city walls, north of the graveyard. The other one, much better preserved, enters the city through Lefke gate (Fig. 6). The best-preserved parts of this aqueduct extend along 600 m, starting from the city gate, with an E-W orientation. 1 km east of the city, the aqueduct runs along the southern border of a carbonate massif where its sources are located (Dereköy village, see Fig. 3a for location). The aqueduct presents an underground section, 400 m long. The aqueduct of Iznik has only recently been studied in detail by Benjelloun et al. (2018). Using a stratigraphic approach coupled with architectural analogies, they concluded that the earliest phases visible were likely to belong to Justinian's period (6th century AD), and identified major restoration works around the 11th and 13th centuries AD.

The walls of Iznik

The defensive walls of Iznik are made of two belts surrounding the city (Fig. 6b). They were extensively studied by Schneider and Karnapp (1938) and Foss and Winfield (1986) (the chronology of the fortifications is presented in Fig. S1 in the electronic supplement). The inner belt was first built during the 3rd century AD, after Gothic attacks in 256-257. The remains of these early walls can still be seen at several points (Fig. 4b).

After an Arab attack in 727, the walls were partly rebuilt by Leo III (717-741). These reconstructions mainly affected the eastern and southern parts. Another important reconstruction campaign followed in 858 under Michael III, especially affecting the eastern and southern sides. After a period of peace, the 10th and 11th century saw the walls damaged on several occasions, until the city was taken by the Turks in the end of the 11th century. In 1097, the city was given back to the Byzantine ruler Alexios I Komnenos, who carried out a few reconstructions (Fig. 4a). The last major reconstructions occurred

during the Lascaris and Palaeologue periods in the 13th century (Fig. 4c), with the addition of the outer walls during the reign of John III Doukas Vatatzes (1222-1254 AD). Since 2018, important restoring works have been carried out on the defensive walls, erasing most of the traces of previous damage and reconstruction phases. Our observations on the walls were done before the beginning of these works.

Intra muros buildings

We inventoried several deformations and possible "seismoresistant" techniques in the Iznik theater (Fig. 6b), built during the 2nd century AD, and spoiled significantly as a quarry in later periods. Deformations were also described in Aya Sofia, a church built by Justinian in the 6th century AD, restored in the 9th, 11th, and 13th centuries, and converted into a mosque by Orhan shortly after the Ottoman conquest of 1331 (Brounoff, 1925; Schneider, 1943). We also found deformations and technical innovations potentially related to earthquakes in several Ottoman buildings: Yesilcamii mosque built in the late 14th century (Fig. 4e), Mahmut Celebi mosque built in 1442, and Murat II hamam built in the first half of the 15th century (Fig. 4d). Other traces of damage were encountered on a few Ottoman tombstones located in Candarli Hayrettin Pasa mausoleum.

DAMAGE INVENTORY

Location of the damage

We inventoried 235 cases of damage (Fig. 5). The observations are especially dense on the inner walls (almost 4 observations every 100 m in average) and the outer walls seem much less affected (less than 1 observation every 100 m on average). The damage observed is in general regularly distributed all along the inner walls. In some areas the density of observations is much lower. This can be the case when the remains have disappeared, such as in west of the city. In other areas, the dense vegetation

214 or the presence of private areas near the walls prevented the survey, such as in the northeastern
215 section between towers 46 and 50, and in the southwestern section between towers 95 and 104.

216 ***Azimuth of the damaged walls***

217 The relative repartition of the different wall orientations was compared to the relative number of EAE
218 found in these different wall azimuth ranges, no matter the azimuth of the deformation (Fig. 8a). The
219 results do not change significantly when data of lower qualities are included. If all the walls were
220 affected in the same way whatever their azimuth, the relative amount of EAE and the orientations
221 should present similar distributions. This is the case for the E-W and NW-SE oriented walls that show
222 a correspondence between the relative amounts of EAE and the lengths of the walls affected. By
223 contrast, we can see that the N-S oriented walls bear much more EAE than what could be expected
224 from their length: they contain a third of the walls' EAE whereas they represent only 12.7% of the total
225 wall length. Conversely, the NE-SW oriented walls are underrepresented in terms of EAE.

226 ***Oriented deformations***

227 105 of our observations present an oriented pattern (e. g. azimuth of collapse or expulsion). Most of
228 the oriented deformations show a strong correlation with the wall azimuth (Fig. 8b): they are either
229 perpendicular to the wall (out-of-plane) or parallel (in-plane). A clear, dominant, N-S azimuth appears,
230 representing 30% of the observations (Fig 8c). This actually mirrors the greater length of walls oriented
231 E-W (Fig. 8a). For almost all the azimuth ranges, deformations exist in both directions, but the
232 deformations oriented NE-SW are characterized by an exclusive NE strike of the damage.

233 ***Time constraints on the deformations***

234 The earliest EAE are found almost all around the inner walls and in the theater (Fig. 5b). The later
235 sections of the walls were also affected by several deformations. The aqueduct shows a significant
236 number of EAE from all periods. EAE from the Ottoman period were found especially intra muros on
237 the mosques and the bathhouse. It is expected that older buildings display a larger amount of damage

compared to more recent ones because they are more likely to accumulate damage from several deformation episodes. As mentioned in the previous section, the amount of EAE seems much smaller on the outer walls built in the 13th century, which is coherent with the fact that it is one of the latest buildings of the Byzantine period.

The repairs were mainly dated relying on the age of the repaired structure and the technique used in the repair. We could find repairs for all the major construction periods of the city, from the 9th century to the Ottoman times (for the list, see Table S3 in the electronic supplement). For the earlier periods, we could only find possible seismoresistant techniques of construction in the theater with the use of polygonal imbricated ashlars (Garduño-Monroy et al., 2012; Hinzen and Montabert, 2017).

We were also able to date with ^{14}C four charcoal samples from mortar filling the dismantled ashlars of tower T57 base and one sample from the new masonry covering the rotated blocks of Istanbul Gate (Fig. 4f, see Fig. 6b for locations). The ages obtained point toward repairs following a deformation episode in the late 11th or early 12th centuries (Table 1). Finally, we tried to date the organic fraction of carbonate concretions sampled on the aqueduct wall, but we obtained a very recent age. The link between the external concretions and historical earthquakes is therefore unlikely.

Combining the ages of the affected walls and their repairs, we obtain many time ranges of different widths constraining one or several events (Table 2). The narrower, distinct time intervals obtained for possible earthquakes are (1) 527-787, (2) 858-1097, and (3) after the late 14th century AD. The first interval corresponds to several good quality EAE but located in Aya Sofya only. The second interval is constrained by one intermediate and one bad quality EAE in the walls, but also matches the ^{14}C ages of the sampled postseismic repairs. It is then probable that the associated damage observed on Istanbul Gate and tower T57 belongs to this episode. The third interval is documented by one good and two intermediate quality EAE in the walls. We can also mention a wider interval, between 730 and 1254 AD, including 12 good quality EAE that might belong to the two precedent intervals. Finally, the Ottoman period presents 17 EAE, mostly of good quality, collected on four different buildings. The

earliest building, Yesilcamii, was built in 1378 AD, but the EAE observed on Celebi camii indicate a deformation occurring after 1442 AD.

Vulnerability analysis and estimation of local intensity

The investigated buildings were classified into three vulnerability classes A, B and C following the EMS-98 framework (Grünthal & Levret, 2001). Class A includes the most vulnerable buildings, which use rough rubble stones and a mortar of average quality. Class B includes the buildings using carefully cut stones or terracottas, and a mortar of good quality. Class C includes more resistant buildings using large ashlar. When the building presented visible defaults or weaknesses in its construction, we lowered its vulnerability class by one rank (e.g. A instead of B). For each vulnerability class, we computed the ratio of the total number of damage of a given grade observed over the length of the walls considered (Fig. 9a). The damage repartition is quite similar for classes B and C with a maximum for grade 2 (moderate) and limited damage for higher grades. The buildings of class A appear less affected by individual cases of damage on their total length, but are characterized by a higher severity of the damage, with a maximum for grade 3 (important non-structural damage and moderate structural damage).

The assessment of building damage following an earthquake makes it possible to derive a local intensity reflecting the severity of ground shaking. For that, the damage distributions obtained for different building vulnerability classes is compared to empirical relationships (damage probability matrices, DPM) linking, for a given intensity, the probability that buildings are affected by damage of different grades (Fig. 9b; Riedel, 2015). In modern postseismic damage surveys, each building is given one grade of damage. In our case, the number of individual buildings that could be surveyed is too low, and long linear buildings like the defensive walls and the aqueduct cannot be considered “individual buildings”. Therefore, we chose to assign a damage grade to each EAE and to consider the ratio of EAE per linear meter of wall. It is difficult to directly compare our damage ratios with the DPMs because

our counting method should be first calibrated with modern earthquakes, but we can still obtain qualitative estimates of intensity.

For vulnerability class A, we obtain a flat distribution for quality 1 EAE (Fig. 9a). When lower qualities are included, we observe a larger peak for grade 3 damage and a significant representation of grade 1 damage. The grade 3 damage peak points toward a VII-VIII intensity, but our grade 1 damage is overrepresented compared to the DPM in this range. For vulnerability class B, the obtained distribution is more regular and insensitive to EAE quality, with a maximum for grade 2 followed by a progressive decrease for bigger grades. This distribution is most compatible with an intensity VIII. For vulnerability class C, we obtain a similar distribution to class B, with a clear maximum for grade 2 and much lower ratios for the other grades. This suggests a VIII-IX intensity, with an overrepresentation of grade 4 damage compared to the DPM in this range. As a result, a minimal intensity VIII seems to account best for the three damage distributions (Fig. 9b).

MODELING OF THE DEFORMATION OF THE OBELISK

The obelisk located north of Iznik was chosen to test numerically whether an earthquake rupturing the MNAF is able to cause the displacement of the blocks, as is observed today. The constituting elements of the obelisk were measured in order to build a 3D model of the obelisk (for the geometry of the model, see Fig. S2 in the electronic supplement). The numerical model was built using a non-linear transient finite-element analysis (Baillet et al., 2005). The marble blocks were assigned a Young modulus of 50 GPa, a Poisson's ratio of 0.2 and a density of 2.7. Two values of Coulomb friction coefficient between each block were tested at 0.5 and 0.7. We selected as input five three-component ground acceleration signals, recorded during four real strike-slip earthquakes (for the list and characteristics of these earthquakes, see Table S5 in the electronic supplement). The range of magnitude of these earthquakes is Mw 5.9-7.3. The signals were selected so that the distance between the recording station and the epicentre was in the same range as the distance between the obelisk and

312 the closest MNAF segments (5-20 km) and with a similar site effect category (site class C in Eurocode-
313 8). The acceleration signals were converted into displacement signals with two integrations. Before
314 each integration, we subtracted the mean and the trend to prevent a drift of the signals, and smoothed
315 the high-frequency peaks with a 4-order bandpass Butterworth between 0.1 and 20 Hz. The signals
316 were eventually resampled to the 0.5e-5 s time step of the numerical modeling approach. They were
317 then imposed at the base surface of the obelisk. In a second set of simulations, we applied the
318 earthquake signals twice in a row to reproduce examples of cumulative deformation (Fig. 10).

319 Most of the energy of the seismic signals is focused below 1 Hz for the Düzce earthquake and 4 Hz for
320 the others. The modal analysis of the modeled structure shows two main resonance frequencies at 7.8
321 and 7.84 Hz in flexional modes. The third mode corresponds to a frequency over 30 Hz, which is not
322 excited by the selected seismic signals.

323 The obelisk collapses only for the signal of Mw 7.3 Düzce earthquake (Table 3). For the other signals,
324 the obelisk still shows irreversible relative displacement between blocks. The most significant values
325 of displacement between adjacent blocks are obtained for the Mw 6.1 Azores Islands and Mw 5.9
326 Kyllini signals. At the end of the single-event simulations, these values are slightly lower than the
327 centimeter offsets observed on the field. The relative rotations obtained between adjacent blocks are
328 less than 1° and hardly reproduce the actual rotation component, clearly visible on the monument. At
329 the end of the double-event simulations, the obelisk remains standing for all events but Düzce, and
330 shows a cumulative deformation, which is twice the deformation of the single-event simulations. The
331 final values obtained for two Azores Islands events better reproduce the field observations.

332

333

334

335

DISCUSSION

Local intensity and associated earthquakes

Our intensity estimation can be impacted by two biases. (1) Contrary to postseismic surveys, we did not study a representative sample of the buildings that used to stand in Iznik in ancient and medieval times. It is probable that the buildings still visible today are among the most resistant, and that the more vulnerable buildings have disappeared and were replaced by modern constructions. The empirical damage distributions suggest that the heaviest structural damage is concentrated on these vulnerable buildings, while the more resistant buildings tend to mainly bear slighter damage (Fig. 9b). Therefore, the successive cycles of repairs and reconstructions will tend to erase the traces of the heaviest damage (grades 4 and 5), while the slighter damage will be preferentially preserved. This selection bias will lead to underestimation of the intensity felt in Iznik during past earthquakes. This means that we constrain a minimal intensity. (2) Our damage dataset results from the cumulative effects of several earthquakes, and our qualitative comparison with the DPMs relies on the assumption that these earthquakes produced similar damage distributions. This seems to be the case as the obtained damage distributions are close to the empirical DPMs (Fig. 9). We can also assume that the final curve will mostly reflect the bigger events, which leave most traces of damage. Our vulnerability analysis may thus only constrain a minimal intensity, around VIII, for the biggest ruptures suffered in Iznik in the last two millennia.

With an epicentre located on the fault segments 3 km south of the city on the MNAF segments, an intensity VIII in Iznik can be produced by a Mw 6+ earthquake (Erdik et al., 1985). The deformations observed on the obelisk suggest magnitudes over 6, probably between 6 and 7, in the case of events rupturing the same segments south of Iznik, in agreement with the vulnerability analysis. However, the modeling also shows that a stronger earthquake near Iznik would have destroyed the obelisk. We may therefore rule out the occurrence of this kind of Mw 7+ event during the historical period for the fault segments close to Iznik.

361

362 ***Historical seismicity scenarios***

363 The vulnerability analysis and obelisk modeling argue for a significant seismogenic potential of the
364 MNAF. In this section, we discuss the deformation episodes identified by archeoseismology and
365 examine together independent evidence gathered from the historical seismicity catalogues and
366 paleoseismic trenching studies.

367 *Possible deformations before the 6th century AD*

368 Although it was not possible to find repairs anterior to the 8th century AD, a part of the EAE affecting
369 the older buildings of Iznik may have been caused by earlier earthquakes. The historical catalogue
370 includes six events with damage reported in Nicaea (Fig. 2). Three events were attributed to the MNAF,
371 in 29-32 AD, 121 AD and 368 AD. The magnitudes estimated are around 7 and it seems that the 121
372 AD event was the strongest, possibly of M~7.4. While the first two events are said to have caused
373 partial destruction in Iznik, the 368 AD event is said to have caused complete destruction. This last
374 description is likely exaggerated as several buildings from this period, such as the theater and the 3rd
375 century walls, are still standing today.

376 We also need to examine the possibility that Nicaea was affected by earthquakes rupturing the NNAF.
377 Historical descriptions do include such occurrences, e. g. in 358 AD, 362 AD and 478 AD with
378 magnitudes estimated between 6.8 and 7.4, but the precise nature and severity of the destruction
379 caused are difficult to determine (Fig. 2). A Mw 7.5 earthquake rupturing the fault segments crossing
380 Izmit Gulf may produce an intensity VIII in Iznik (Erdik et al., 1985). However, during the 1999 Mw 7.6
381 Izmit earthquake, intensities VI were reported in the Iznik area and the local seismic station recorded
382 a peak horizontal acceleration of 0.12g only (Celebi et al., 2000). Accordingly, the damage in Iznik was
383 slight: the chimneys of some houses fell down or were bent and a very small part of the defensive walls

collapsed (pers. comm. Cengiz Celik). Therefore, the earthquakes rupturing the NNAF are unlikely to account for a significant part of our damage dataset.

The 527-787 AD episode

This period of time is associated with two historical earthquakes, both of them located on the NNAF (Fig. 2). In 554 AD, a Ms~7 earthquake severely affected Constantinople and Nicomedia (Izmit). Partial damage is reported in Iznik, but by one source only. In 740 AD, a major Ms 7.1 event affected the eastern part of the Marmara Sea and it is reported that "a single church survived" in Iznik which was totally destroyed. For the same reasons as exposed above, this testimony cannot be taken literally. But given that no other earthquake is known in the region, the EAE associated to this episode may result from these earthquakes. It should be emphasized that our constraints for this episode are scarce and limited to one building only.

The 858-1097 episode

Iznik was affected by war damage during this period of time. In the late 10th century, the Byzantine general Bardas Skleros led a wide-scale rebellion in Asia Minor. In 978, he besieged Iznik and some parts of the walls, especially the tower T106 in the southwest were heavily damaged (Holmes, 2005). One century later, the city was temporarily seized by the Turks and was attacked by the Crusaders in 1097 AD. Most fights happened around the southern gate, damaging the walls and destroying tower T106 (Cahen, 1948; Foss, 1996; Norwich, 1993).

Our evidence for this deformation episode includes good quality EAE and rebuilding on tower T57 and Istanbul Gate in the northern section. The rebuilding closely postdates the only historical earthquake documented in Iznik for this time interval, in 1065 AD. With a magnitude estimated at 6.8, it caused widespread damage to churches, the city walls, and numerous houses. No other locality seems to have been damaged, which suggests a local event rupturing the MNAF. Sediment cores recently sampled in the southeastern part of Iznik Lake corroborate the occurrence of a seismic event rupturing the fault

segments south of Iznik during the 11th century AD (Gastineau et al., 2020 PREPRINT). We can consider that our EAE dataset most probably includes the archeological signature of this event.

The Ottoman episode (after 1330 AD)

The traces of earthquake damage found on several Ottoman buildings indicate that Iznik was affected by at least one significant earthquake since the 14th century AD. Three different scenarios can be proposed.

(1) This damage may have resulted from earthquakes rupturing the NNAF. Several historical earthquakes with damage reported at Iznik are known (Fig. 2). In 1754 AD, a strong Ms 7 earthquake affected the region of Izmit on the NNAF, destroying a few houses in Iznik, apparently without casualties. In 1878 and 1893 AD, two smaller earthquakes in the same area of the NNAF caused slight damage in Iznik, but with much lower magnitudes, between 5 and 6. Finally, in 1894 AD, a Ms 7.3 earthquake ruptured the Izmit Gulf faults and caused liquefaction and landslides in the epicentral region and widespread destruction between Istanbul, Gemlik and Sapanca. The effects in Iznik are not well known.

(2) Another source of damage comes from a cluster of earthquakes that affected the SNAF and MNAF west of Iznik in the second half of the 19th century (Fig. 2). Most of the activity extended between Bursa and Gemlik, but it seems that some ruptures were also located closer to Iznik, probably along the faults bordering the southern shore of Iznik Lake. The biggest earthquakes happened in the Bursa region and did not affect the area east of Gemlik significantly. The other events correspond to much smaller earthquakes, with magnitudes under 6. Only slight damage is mentioned in Iznik on March 3, 1893 AD.

(3) Interestingly, the Ottoman episode matches the paleoseismic evidence of two contemporary ruptures (Fig. 2), sometime between the 12th and 18th century AD in Gemlik (Özalp et al., 2013), and sometime between the 14th and 18th century AD in the west of Mekece (Ikeda, 1988). It can thus be proposed that the Ottoman damage in Iznik was caused by one or several earthquakes rupturing the

MNAF segments between the 14th and 18th centuries AD. The trench data do not constrain the magnitudes of these events, but the obelisk modeling argues against a Mw 7+ earthquake south of Iznik, which suggests more moderate and/or distant events. The historical catalogues do not present any mention of Iznik between the 12th and 18th centuries AD, but it can be questioned whether this reflects a true period of seismic quiescence for the Iznik region. It is known that at the end of the 13th centuries, Iznik suffered significant emigration because of the Ottoman conquests in Anatolia, so much so that after the city was conquered, in 1331 AD, it was described as a ruined city only inhabited by few people (Ibn Batuta, 2012). The city eventually lost its political and strategic importance, which might explain why it disappeared from the archives of past seismicity. In comparison, important centers like Bursa or Gemlik continued to suffer damage from repeated earthquakes, such as in 1419 AD. During this period of time, the historical catalogue also includes events which were felt in Istanbul but with too little information to precisely locate the epicenter, e.g. in July 1402 and January 1656 AD (Ambraseys, 2009).

CONCLUSION

Using an archeoseismological approach, we identified 235 traces of possible earthquake damage in Iznik, and more than 100 of them can be attributed to seismic shaking with high confidence. The different walls of the city, depending on their orientation or their age, show different patterns of damage. The damage was more severe for N-S oriented walls, while NE-SW walls show less deformation. The older constructions are also more affected than more recent walls. Three distinct episodes of earthquake damage were identified, two before the Ottoman conquest of 1331 AD, and one after. The dating of several repairs associated with earthquake damage enabled us to constrain the time of occurrence of two individual events, between 527 and 787 AD, and between 858 and 1097 AD. While the latter event may correspond to the 1065 earthquake described by ancient sources, the two others can be accounted for by different earthquake scenarios. We have estimated that the

damage observed corresponds to a minimal intensity VIII, most compatible with ruptures along the MNAF segments of magnitudes above 6. The modeling of an obelisk a few kilometres north of Iznik also suggests magnitudes over 6, but is incompatible with a stronger, Mw 7+ rupture along the MNAF segments south of Iznik. This last result implies that the fault segments south of Iznik have not known a big rupture for nearly two millenia, which corresponds to several meters of accumulated stress. This study shows that in favourable contexts, archeoseismology can be used complementarily with historical seismology and paleoseismology to refine past earthquake scenarios and contribute to a better seismic hazard assessment.

Data and Resources

The bathymetric map of Marmara was made available by the EMODnet Bathymetry project, (https://www.emodnet.eu/bathymetry), using the EMODnet Bathymetry portal (EMODnet Bathymetry Consortium (2016): EMODnet Digital Bathymetry (DTM), http://doi.org/10.12770/c7b53704-999d-4721-b1a3-04ec60c87238) funded by the European Commission Directorate General for Maritime Affairs and Fisheries. The large-scale topography of the study area was obtained from the Shuttle Radar Topography Mission 1 Arc-Second Global (DOI: /10.5066/F7PR7TFT). The bathymetry of Iznik Lake was provided by and can be obtained from the Turkish General Directorate of Hydraulic Works (DSI). The raw acceleration signals can be obtained from the Engineering Strong Motion Database (https://doi.org/10.13127/ESM.2; Luzi et al., 2020). The EAE photos, the 3D displacement signals used as input for the obelisk modeling and the complete output file can be obtained on the Zenodo repository at https://zenodo.org/record/3966773. The maps of Figures 5 and 6 are from Google Earth satellite imagery. The diagrams of Figures 8 and 9 were prepared using the Matplotlib 3.3.0 package for Python (https://matplotlib.org/; Hunter, 2007). Supplemental Material for this article includes the lists of mentioned historical earthquakes and EAE,

additional information on the walls chronology and obelisk model, and the complete data of wall orientations.

Acknowledgements

The authors thank the editors and the reviewer for their helpful comments and suggestions. This work has been supported by the MISTRALS-ENVIMED program (NAFIGEA project), the INSU ALEAS program (France), Labex OSUG@2020 (Investissements d'avenir – ANR10 LABX56, France), and ANR CE03-2019 Basiliznik-secrets. This study contributes to the IdEx Université de Paris ANR-18-IDEX-0001. We thank the Turkish Ministry of Culture and Tourism for allowing the field work. We are also grateful to Mustafa Aktar and Cengiz Celik from Boğaziçi University Department of Geophysics, and to the students from Bursa University Department of Archaeology for their help during the field data acquisitions.

References

Ambraseys, N. (2000). The Seismicity of the Marmara Sea Area 1800-1899, *J. Earthquake Eng.* **4** 377–401.

Ambraseys, N. (2002). The Seismic Activity of the Marmara Sea Region over the Last 2000 Years. *Bull. Seism. Soc. Am.* **92** 1–18.

Ambraseys, N. N. (2009). *Earthquakes in the Mediterranean and Middle East. A multidisciplinary study of seismicity up to 1900*, Cambridge, 968 p.

Ambraseys, N. and C. Finkel (1991). Long-term seismicity of Istanbul and of the Marmara Sea region, *Terra Nova* **3** 527–539.

Ambraseys N.N. and J. A. Jackson (1998). Faulting associated with historical and recent earthquakes in the Eastern Mediterranean region, *Geophys. J. Int.* **133** 390-406.

Ambraseys, N. and J. A. Jackson (2000). Seismicity of the Sea of Marmara (Turkey) since 1500, *Geophys. J. Int.* **141** F1.

Baillet, L., d'Errico, S., and Y. Berthier (2005). Influence of sliding contact local dynamics on macroscopic coefficient variation, *Revue Européenne des Eléments Finis* **14** 305-321.

Barka, A. (1992). The North Anatolian fault zone, *Annales Tectonicae* **6** 164–195.

Barka, A. (1993). Kuzey Anadolu Fayı'nın Sapanca-Izmit ve Geyve-Iznik Kolları üzerinde Paleosismik Arastırmalar. Technical report, TÜBITAK, Istanbul. Proje No:YBAG- 4/7551.

Benjelloun, Y., de Sigoyer, J., Dessales, H., Garambois, S., and M. Sahin (2018). Construction history of the aqueduct of Nicaea (Iznik, NW Turkey) and its on-fault deformation viewed from archaeological and geophysical investigations, *J. Archaeol. Sci Reports* **21** 389-400.

Bilham, R., Gaur, V. K., and P. Molnar (2001). Himalayan seismic hazard, *Science* **293** 1442–1444.

Bronk Ramsey, C. (2009). Bayesian analysis of radiocarbon dates, *Radiocarbon* **51** 337–360.

Brounoff, N. (1925). L'église de Sainte-Sophie de Nicée, *Echos d'Orient* **24** 471-481.

Cahen, C. (1948). La Première Pénétration Turque en Asie Mineure, *Byzantion* **18** 5-67.

Celebi, M., Toprak, S., and T. Holzer (2000). Strong-Motion, Site-Effects and Hazard Issues in Rebuilding Turkey: in Light of the 17 August, 1999 Earthquake and its Aftershocks, in *The 1999 Izmit and Düzce Earthquakes: preliminary results* Barka, A., Kozaci, Ö., Akyüz, S., Altunel, E. (Editors), Istanbul Technical University, 247-263.

Dogan, B. (2010). Kuzey Anadolu Fay Sistemi Güney Kolunun Geyve-Gemlik Arasindaki Kesiminin Morfotektonik, Tektonostratigrafik ve Paleosismolojik Evrimi. PhD thesis, Istanbul Teknik Üniversitesi.

524 Dogan, B., Tüysüz, O., and F. B. Sanli (2015). Tectonostratigraphic evolution of the basins on the
525 southern branch of the North Anatolian Fault System in the SE Marmara Region, Turkey, *Int. J. Earth*
526 *Sci.* **104** 389-418.

527 Emre, Ö., Duman, T., Y., and S. Özalp (2011). 1:250.000 Ölçekli Türkiye Diri Fay Haritası Serisi, Bursa
528 (NK 35-12) Paftası. Seri No: 9, Maden Tetkik ve Arama Genel Müdürlüğü, Ankara.

529 Erdik, M., Doyuran, V., Akkas, N, and P. Gulkan (1985). A Probabilistic Assessment of the Seismic
530 Hazard in Turkey, *Tectonophysics* **117** 295-344.

531 Ergintav, S., Reilinger, R. E., Cakmak, R., Floyd, M., Cakir, Z., Dogan, U., King, R. W., McClusky, S., and
532 H. Özener (2014). Istanbul's earthquake hot spots: Geodetic constraints on strain accumulation along
533 faults in the Marmara seismic gap, *Geophys. Res. Lett.* **41** 5783-5788.

534 Foss, C. (1996). *Nicaea: A Byzantine Capital and Its Praises*, Holy Cross Orthodox Press.

535 Foss, C., and D. Winfield (1986). *Byzantine Fortifications: An Introduction,* University of South Africa
536 Press, Pretoria, 298 p.

537 Garduño-Monroy, V. H., Benavente Escobar, C., Oliveros, A., Rodriguez Pascua, M. A., Perez Lopez, R.,
538 and J. L. Giner (2012). Evidence of past seisms in Cusco (Peru) and Tzintzuntzan (Mexico): cultural
539 relations, *3rd INQUA-IGCP-567 International Workshop on Active Tectonics, Paleoseismology and*
540 *Archaeoseismology*, Morelia, Mexico.

541 Gastineau, R., de Sigoyer, J., Sabatier, P., Fabbri, S. C., Anselmetti, F. S., Develle, A. L., Sahin, M.,
542 Gündüz, S., Niessen, F., Gebhardt, A. C. (2020). Active subaquatic fault segments in Lake Iznik along
543 the middle strand of the North Anatolian Fault, NW Turkey. Preprint at
544 https://doi.org/10.1002/essoar.10504104.1

545 Grünthal, G., and A. Levret (2001). L'échelle macrosismique européenne. *Conseil de L'Europe* -
546 *Cahiers du Centre Européen de Géodynamique et de Sismologie* **19**.

547 Guidoboni, E., Comastri, A., and G. Traina (1994). *Catalogue of ancient earthquakes in the*
548 *Mediterranean area up to the 10th century*, Istituto Nazionale di Geofisica.

549 Guidoboni, E. and Stucchi, M. (1993). The contribution of historical records of earthquakes to the
550 evaluation of seismic hazard, *Annals of Geophysics* **36** 201-215.

551 Hinzen, K.-G. (2005). The Use of Engineering Seismological Models to Interpret Archaeoseismological
552 Findings in Tolbiacum, Germany: A Case Study, *Bull. Seism. Soc. Am.* **95** 521–539.

553 Hinzen, K. G., and A. Montabert (2017). Rectangular Blocks vs Polygonal Walls in Archaeoseismology,
554 *Annals of Geophysics* **60** S0443.

555 Holmes, C. (2005). *Basil II and the Governance of Empire, 976-1025*, Oxford University Press, Oxford.

556 Hubert-Ferrari, A., Barka, A., Jacques, E., Nalbant, S. S., Meyer, B., Armijo, R., Tapponnier, P., and G. C.
557 P. King (2000). Seismic hazard in the Marmara Sea region following the 17 August 1999 Izmit
558 earthquake, *Nature* **404** 269-273.

559 Hunter, J. D. (2007). Matplotlib : A 2D Graphics Environment, *Comput. Sci. Eng.* **9** 90-95.

560 Ibn Batuta (2012). *Voyages d'Ibn Batoutah: Texte Arabe, accompagné d'une traduction (Vol. 4)*.
561 Defrémery, C., Sanguinetti, B. R. (Editors), Cambridge University Press, Cambridge.

562 Ikeda, Y. (1988). Recent activity of the Iznik-Mekece fault at Corak stream, east of Iznik, in
563 *Multidisciplinary research on fault activity in the western part of the North Anatolian fault zone*
564 Honkura, Y., Isikara, A. M. (Editors), Tokyo Institute of Technology, Tokyo, 15-27.

565 Ikeda, Y., Suzuki, Y., and E. Herece (1989). Late Holocene activity of the North Anatolian fault zone in
566 the Orhangazi plain, Northwestern Turkey, in *Multidisciplinary research on fault activity in the western*
567 *part of the North Anatolian fault zone (2)* Honkura, Y., Isikara, A. M. (Editors), Tokyo Institute of
568 Technology, Tokyo, 16-30.

569 Karcz, I. and U. Kafri (1978). Evaluation of supposed archaeoseismic damage in Israel, *J. Archaeol. Sci.*
570 **5** 237–253.

571 Kazmér, M. (2014). Damage to Ancient Buildings from Earthquakes, in *Encyclopedia of Earthquake*
572 *Engineering* Beer, M., Kougioumtzoglou, I., Patelli, E., Au IK. (Editors), Springer, Berlin, Heidelberg.

573 Korzhenkov, A. M. and E. Mazor (1999). Structural reconstruction of seismic events: ruins of ancient
574 cities as fossil seismographs, *Science and New Technologies Special issue* **1** 62–73.

575 Luzi, L., Lanzano, G., Felicetta, C., D'Amico, M. C., Russo, E., Sgobba, S., Pacor, F., and ORFEUS Working
576 Group 5 (2020). *Engineering Strong Motion Database (ESM) (Version 2.0)*, Istituto Nazionale di
577 Geofisica e Vulcanologia (INGV).

578 Mazor, E. and A. Korzhenkov (2001). Applied archaeoseismology: decoding earthquake parameters
579 recorded in archaeological ruins, in *The Makhteshim Country: A Laboratory of Nature* Krasnov, B. and
580 Mazor, E. (Editors), Pensoft Publishers, Sofia- Moscow, 123–149.

581 McCalpin, J. P. (2009). Field techniques in palaeoseismology - terrestrial environments, in
582 *Palaeoseismology* J. P. McCalpin (Editor), Academic Press, 123–149.

583 Michetti, A. M., Audemard, F. A., and S. Marco (2005). Future trends in paleoseismology : Integrated
584 study of the seismic landscape as a vital tool in seismic hazard analyses, *Tectonophysics* **408** 3-21.

585 Norwich, J. J. (1993). *Byzantium: The Apogee*, Penguin.

586 Özener, H., Yilmaz, O., Dogru, A., Turgut, B., and O. Gurkan (2013). GPS-derived velocity field of the
587 Iznik-Mekece segment of the North Anatolian Fault Zone, *J. Geodyn.* **67** 46–52.

588 Özalp, S., Emre, Ö., and A. Dogan (2013). The segment structure of southern branch of the North
589 Anatolian Fault and Paleoseismological behaviour of the Gemlik fault, NW Anatolia, *Bulletin of MTA*
590 **147** 1–17.

591 Öztürk, K., Yaltirak, C., and B. Alpar (2009). The Relationship Between the Tectonic Setting of the Lake
592 Iznik Basin and the Middle Strand of the North Anatolian Fault, *Turkish J. Earth Sci.* **18** 209–224.

593 Pondard, N., Armijo, R., King, G. C. P., Meyer, B., and F. Flérit (2007). Fault interactions in the Sea of
594 Marmara pull-apart (North Anatolian Fault): earthquake clustering and propagating earthquake
595 sequences, *Geophys. J. Int.* **171** 1185-1197.

596 Rapp, G. (1986). Assessing archaeological evidence for seismic catastrophies, *Geoarchaeology* **1** 365–
597 379.

598 Reilinger, R. E., Mcclusky, S. C., Vernant, P., Lawrence, S., Ergintav, S., Cakmak, R., Nadariya, M.,
599 Hahubia, G., Mahmoud, S., Sakr, K., Arrajehi, A., Paradissis, D., Al-Aydrus, A., Prilepin, M., Guseva, T.,
600 Evren, E., Dmitritsa, A., Filikov, S.V., Gomes, F., Al-Ghazzi, R., and G. Karam (2006). GPS constraints on
601 continental deformation in the Africa-Arabia-Eurasia continental collision zone and implications for the
602 dynamics of plate interactions, *J. Geophys. Res.* **111** V05411.

603 Reimer, P. J., Bard, E., Bayliss, A., Beck, J. W., Blackwell, P. G., Bronk Ramsey, C., Buck, C. E., Cheng, H.,
604 Edwards, R. L., Friedrich, M., et al. (2013). IntCal13 and Marine13 Radiocarbon Age Calibration Curves
605 0–50,000 Years cal BP, *Radiocarbon* **55** 1869–1887.

606 Rodriguez-Pascua, M. A., Pérez-Lopez, R., Giner-Robles, J. L., Silva P. G., Garduño-Monroy, V. H., and K.
607 Reicherter (2011). A comprehensive classification of Earthquake Archaeological Effects (EAE) in
608 archaeoseismology : Application to ancient remains of Roman and Mesoamerican cultures, *Quaternary*
609 *Int.* **242** 20-30.

610 Riedel, I. (2015). *Seismic vulnerability analysis of existent buildings. Loss estimation and uncertainty*
611 *analysis for deterministic earthquake scenarios*, PhD thesis, Université Grenoble Alpes.

612 Sahin, M., and M. R. Fairchild (2018). Nicaea's Underwater Basilica, *Biblical Archaeological Review* **44**
613 30-38.

614 Schneider, A. M. (1943). Die römischen und byzantinischen Denkmäler von Iznik-Nicaea, *Istanbuler*
615 *Forschungen* **16**, 40 p.

616 Schneider, A. M., and W. Karnapp (1938). Die Stadtmauer von Iznik (Nicaea), *Istanbuler Forschungen*
617 **9**, 55 p.

618 Sengör, A. M. C. (1979). The North Anatolian Transform Fault: its age, offset and tectonic significance,
619 *J. Geol. Soc. London* **136** 269–82.

620 Sipahioglu, S., and T. Matsuda (1986). Geology and Quaternary fault in the Iznik-Mekece area, in
621 *Electric and Magnetic Research on Active Faults in the North Anatolian Fault Zone* A. M. Isikara and Y.
622 Honkura (Editors), Tokyo Inst. Technology, 25-41.

623 Stein, R. S., Barka, A. A., and J. H. Dieterich (1997). Progressive failure on the North Anatolian fault
624 since 1939 by earthquake stress triggering, *Geophys. J. Int.* **128** 594–604.

625 Wells, D. L., and K. J. Coppersmith (1994). New Empirical Relationships among Magnitude, Rupture
626 Length, Rupture Width, Rupture Area, and Surface Displacement, *Bull. Seism. Soc. Am.* **84** 974-1002.

627 Yoshioka, T., and I. Kuşçu (1994). Late Holocene faulting events on the İznik-Mekece fault in the
628 western part of the North Anatolian fault zone, Turkey, *Bull. Geol. Surv. Jpn.* **45** 677–685.

629

630

631

632

633

634

635

Yacine Benjelloun

Institut de physique du globe - UMR7154

1, rue Jussieu

75238 Paris cedex 05, France

+33 (0)6 80 21 52 44

benjelloun@ipgp.fr

Julia de Sigoyer

Université Grenoble Alpes

ISTerre

CS 40700

38058 GRENOBLE Cedex 9

Julia.de-sigoyer@univ-grenoble-alpes.fr

Hélène Dessales

AOROC – UMR 8546

45 rue d'Ulm

F-75230 Paris cedex 05

helene.dessales@ens.psl.eu

Laurent Baillet

Université Grenoble Alpes

ISTerre

CS 40700

38058 GRENOBLE Cedex 9

Laurent.baillet@univ-grenoble-alpes.fr

Philippe Guéguen

Université Grenoble Alpes

ISTerre

CS 40700

38058 GRENOBLE Cedex 9

Philippe.gueguen@univ-grenoble-alpes.fr

Mustafa Sahin

Uludağ University

Faculty of Arts & Science

Görükle Campus, 16059

Nilüfer, Bursa / TURKEY

mustafasahin@uludag.edu.tr

Table 1: Sample list and radiocarbon dating in Iznik. The dating was done by the LMC14/LSCE. The ages were calibrated with the Oxcal 4.2 program (Bronk Ramsey, 2009) using the IntCal13 calibration (Reimer et al., 2013).

Name	Location	Type	Carbon analyzed (mg)	%modern carbon	^{14}C date (yr BP)	^{14}C calibrated age AD
W5a1	Repair mortar on T57	charcoal	1.38	88.84716	950±30	1024-1155
W5b1	Repair mortar on T57	charcoal	1.25	89.00717	935±30	1026-1162
W5b2	Repair mortar on T57	charcoal	1.33	89.42842	900±30	1039-1210
W5a2	Repair mortar on T57	charcoal	0.09*	87.31807	1090±70	769-1046*
IZAQC2	Aqueduct concretion	tufa	0.79	102.37583	Posterior to 1950	
W61b	Reconstruction Istanbul Kapi	charcoal	1.51	89.36830	905±30	1037-1207

*due to the very low carbon content, this age result has a low confidence level

Table 2: EAE constrained by post-seismic repairs, separated by quality categories.

Terminus post quem	Terminus ante quem	Q1*	Q1+Q2†	Q1+Q2+Q3‡
2nd c.	858	1	1	1
2nd c.	1330	1	1	1
3rd c.	858	5	5	5
3rd c.	1254	6	9	9
3rd c.	1185	2	2	2
3rd c.	1065	0	0	1
3rd c.	1097	11	15	16
3rd c.	1254	7	8	9
3rd c.	1330	0	2	2
527	787	3	3	3
730	1254	12	13	13
858	1097	0	1	2
858	1222	1	1	1
858	1254	0	1	1
858	1330	0	2	2

*Quality rank 1 (good). †Quality rank 2 (average). ‡Quality rank 3 (bad).

684 **Table 3:** Maximum displacements (in mm) and rotations (in °) obtained between adjacent blocks.

Earthquake (station)	Maximum relative displacement (mm)		Maximum relative rotation (°)	
	Friction 0.5	Friction 0.7	Friction 0.5	Friction 0.7
Düzce	Collapse			
Azores Islands	7	7	0.5	0.6
Patti Gulf (PTT1)	1.36	1.3	0.085	0.037
Patti Gulf (MLZ)	0	0	0	0
Kyllini	3	3	0.2	0.19

685

686

687 **List of Figure Captions**

688 **Figure 1:** Morphology and geometry of the NAFZ in the Marmara region. The active fault segments,
689 drawn in black, were taken from Emre et al. (2011) and Benjelloun et al. (2018). The Mw>6.5
690 ruptures during the 20th century are shown in colors (Hubert-Ferrari et al., 2000; Pondard et al.,
691 2007). The main cities are located with dots. NNAF, MNAF and SNAF: northern, middle and southern
692 branches of the NAF.

693

694 **Figure 2:** Chronological frieze of Nicaea's history. The colors show the main historical periods of the
695 city: Roman (blue), Seljuk and Ottoman Turk (green) and Lascarid (yellow). The red stars correspond
696 to historical earthquakes having damaged the city according to historical descriptions, and the white
697 stars indicate the historical events for which the reality or amount of seismic damage is uncertain (for
698 the complete list, see Table S1 in the electronic supplement). The two bars under the frieze refer to
699 earthquakes identified in paleoseismological trenches done on the MNAF.

700

701 **Figure 3:** Field examples of active faulting in the vicinity of Iznik. (a) Shaded DEM of the MNAF
702 region, with the locations of the field photograph. The MNAF segments are mapped in red, and other
703 active faults in black. The lines in the lake correspond to a 5-m interval bathymetry (see Data and
704 Resources). The fault traces in Iznik Lake are taken from Gastineau et al. (2020 PREPRINT). (b)
705 Triangular facets (black arrows) at the southeast corner of Iznik lake. The vertical faulting component
706 of the MNAF is more visible in the landscape in the vicinity of Iznik Lake.

707

708 **Figure 4:** Examples of EAE in Iznik. The white arrows indicate the deformation azimuth and strike. The
709 quality category and identifier are indicated on each picture. (a) Tilted base of the defensive wall, the
710 upper part collapsed and was rebuilt in a very distinct masonry. (b) Conjugated cracks in a vaulted

711 passage of the inner defensive walls. (c) Tower T97, showing a simple terracotta structure from the
712 early 13th century. The crenellations (black dotted line) were blocked (red arrows) during the
713 following reign of John Vatatzes (1222-1254 AD). (d) Arch with imbricated ashlars, bearing traces of
714 damage and posterior cementation on Murat II hamam (early 15th c. AD). (e) Dropped central ashlars
715 on an arch of Yesilcamii mosque (late 14th c. AD). The damaged arches were later reinforced with
716 transversal iron bars, then wood beams. (f) Pushed and rotated ashlars of the inner Istanbul Gate;
717 note the posterior rebuilding in masonry (red arrows). (g) Collapse in the northwestern section of the
718 inner defensive walls.

719

720 **Figure 5:** Inventory and locations of the EAE in Iznik, classified by quality (a) and by age of the wall
721 affected (b).

722

723 **Figure 6:** (a) Satellite image of Iznik surroundings with the active faults drawn in red and the main
724 aqueduct in yellow. (b) Simplified map of Iznik. The historical city is delimited by a double belt of
725 defensive walls and used to be supplied with water by two aqueducts in the east. The other buildings
726 investigated and mentioned in the text are drawn in grey. The numbers refer to the nomenclature of
727 the towers used in the text, following Foss and Winfield (1986).

728

729 **Figure 7:** (a) General view of the obelisk near Elbeyli village. See Fig. 6a for location. (b, c) Detailed
730 views of rotated and offset blocks. The red arrows point to the parts of the pictures where the
731 deformation is most visible.

732

Figure 8: (a) Comparison between the relative distribution of wall length (bars) and quality 1 EAE (line) for different wall azimuths. The percentages in length and EAE were computed on the total wall length and total number of EAE of quality 1, respectively. For the other qualities, see Table S4 in the electronic supplement. (b) Azimuths of the damage plotted against the azimuths of the wall affected. Note the general correlations between the two values. This correlation is linear for the in-plane deformations (i.e. parallel to the wall) and affine with a ±90 shift for the out-of-plane deformations (i.e. perpendicular to the wall). (c) Rose diagrams of the azimuths of damage observed in Iznik (118 EAE). Note the prominent N-S azimuths.

Figure 9: (a) Distribution of the damage of various grades for the three vulnerability classes of buildings in Iznik. (b) Quantitative translations of the EMS98 damage classification according to vulnerability class and macroseismic intensity, adapted from Riedel (2015). The vulnerability class A to C correspond to the buildings studied in Iznik that use terra cotta, rubble and ashlar. The probability distributions of the different damage grades are shown with different colors. For each vulnerability class, we try to find the intensity which best replicates our observed damage distribution (reported on the graphs as vertical bars). For example, for our vulnerability B buildings, we observe a majority of D2 damage. This is compatible with an intensity VII or VIII. Then, the fact that we have much more D3 than D1 damage rather suggests an intensity VIII.

Figure 10: Modeled N displacement (a), E displacement (b), and rotational displacement (c) of the obelisk for the two-event simulation of the Mw 6.1 Azores Islands earthquake. The blocks are numbered from base to top.

Figure 1

Click here to access/download;Figure;Fig1.tif

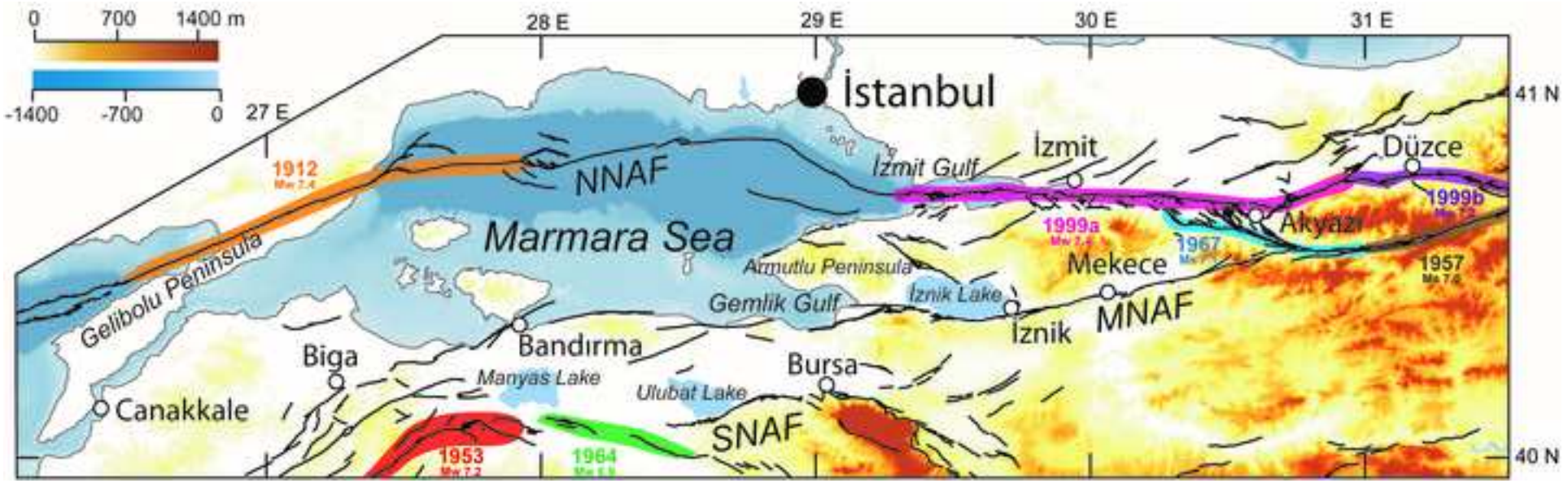

Figure 2

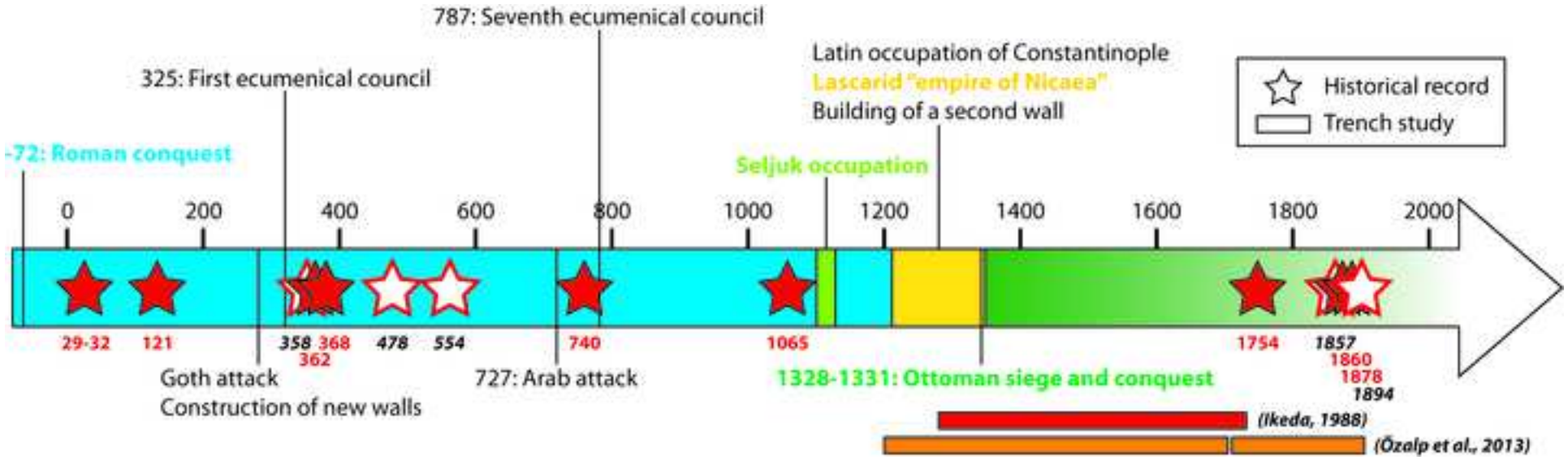

Figure 3

Click here to access/download;Figure;Fig3_crop.tif

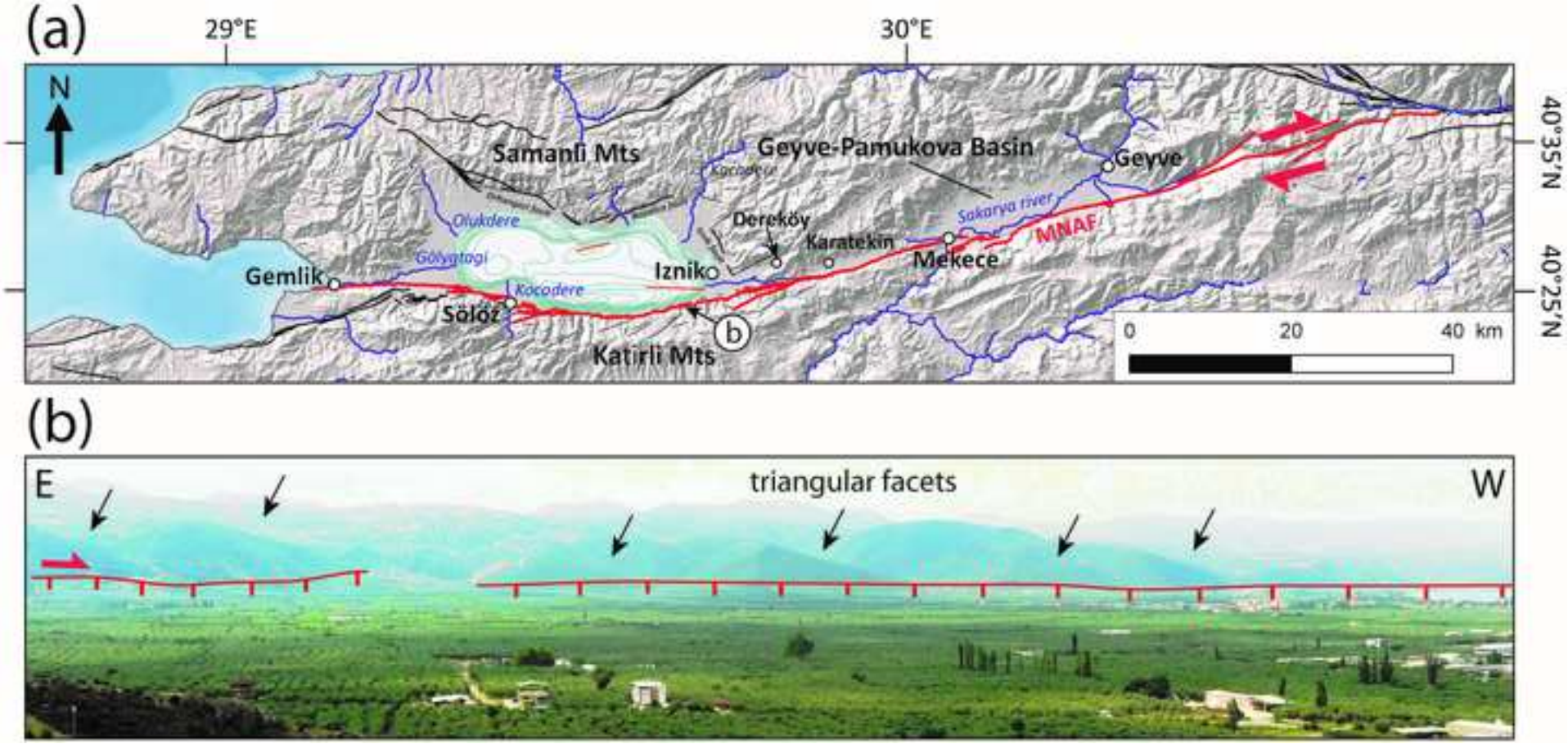

Figure 4

Click here to access/download;Figure;Fig4_300.tif

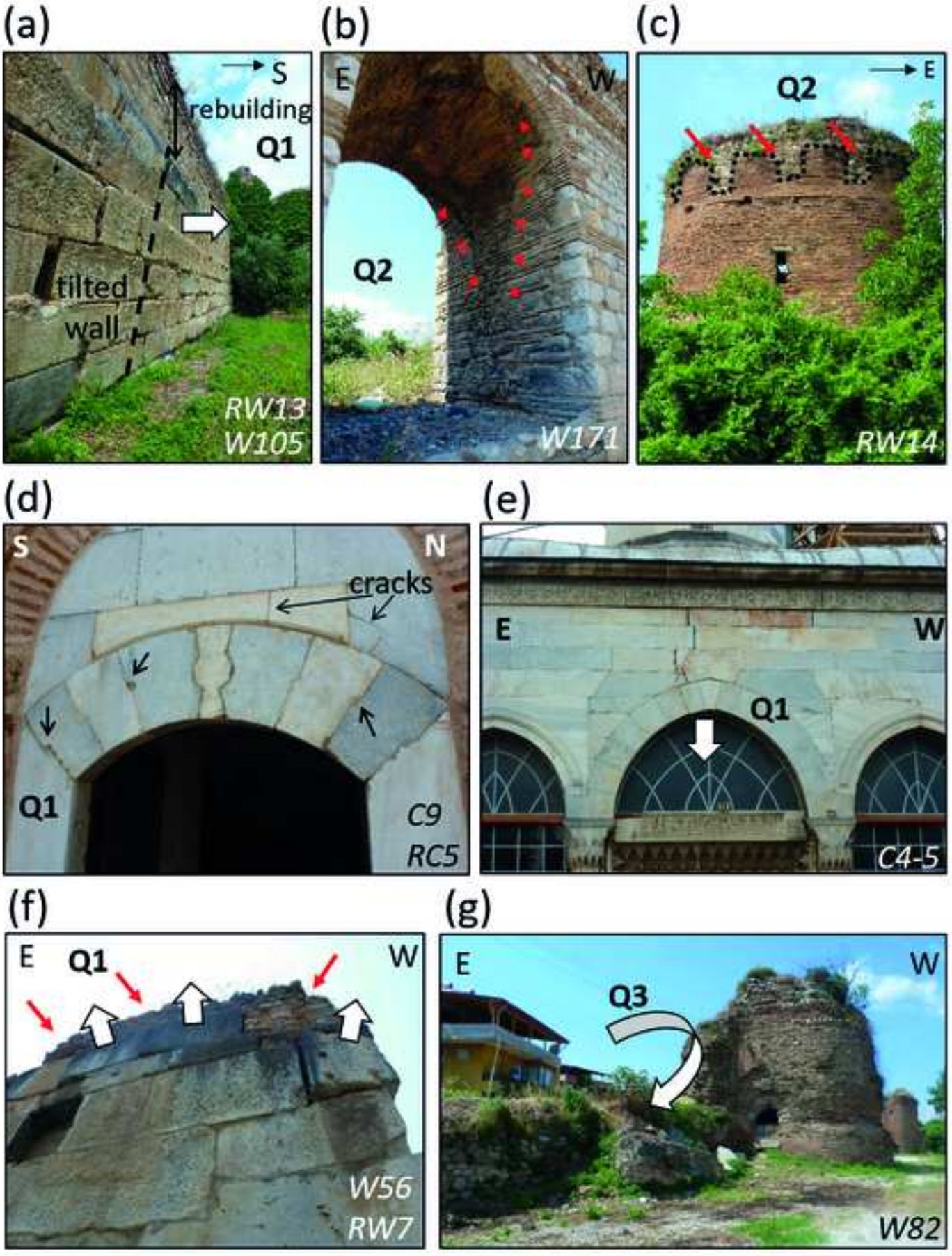

Figure 5

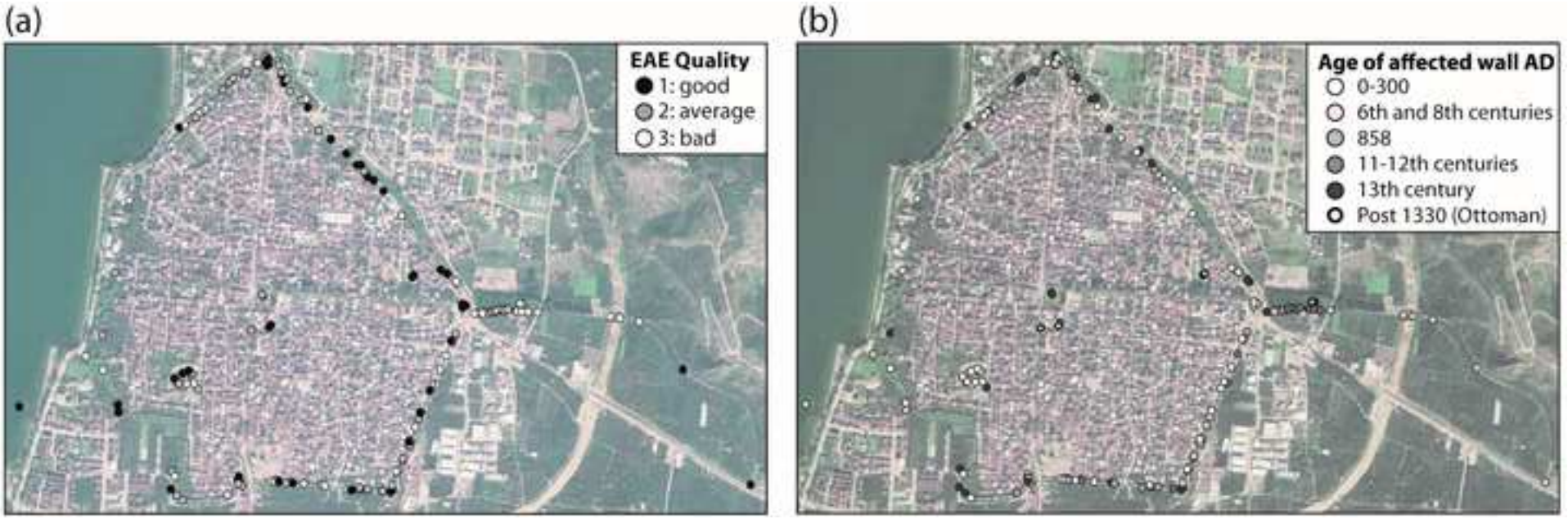

Figure 6

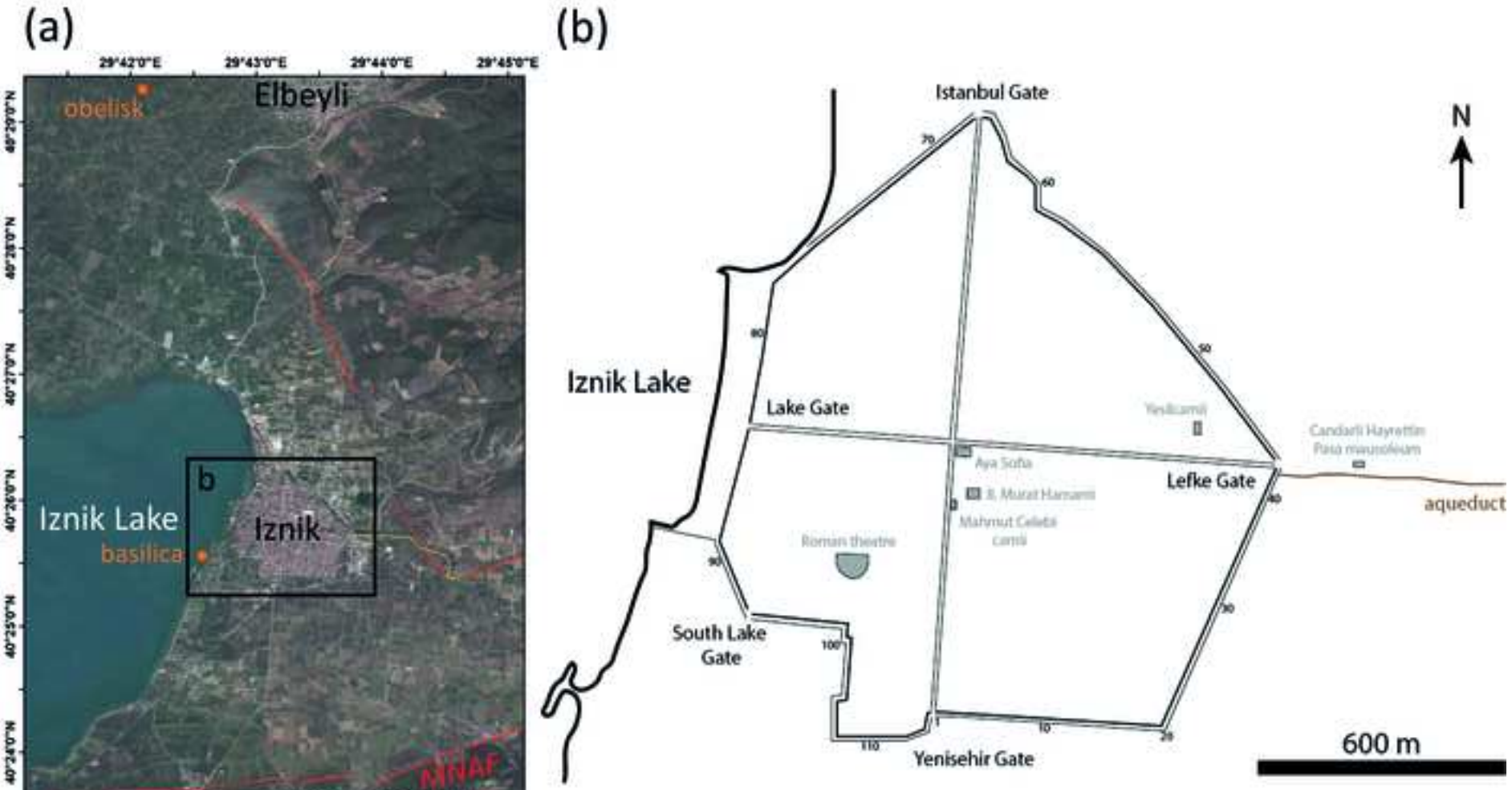

Figure 7

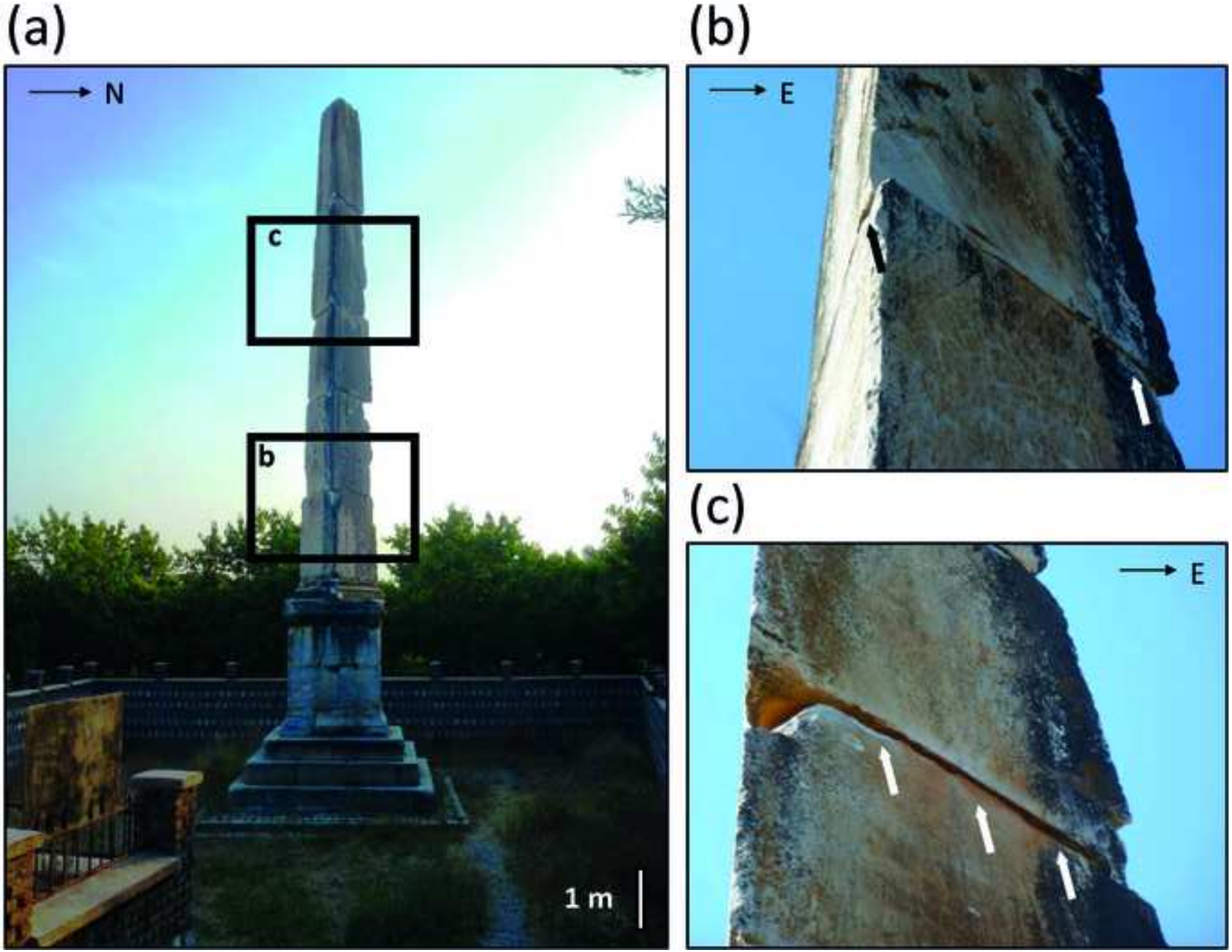

Figure 8

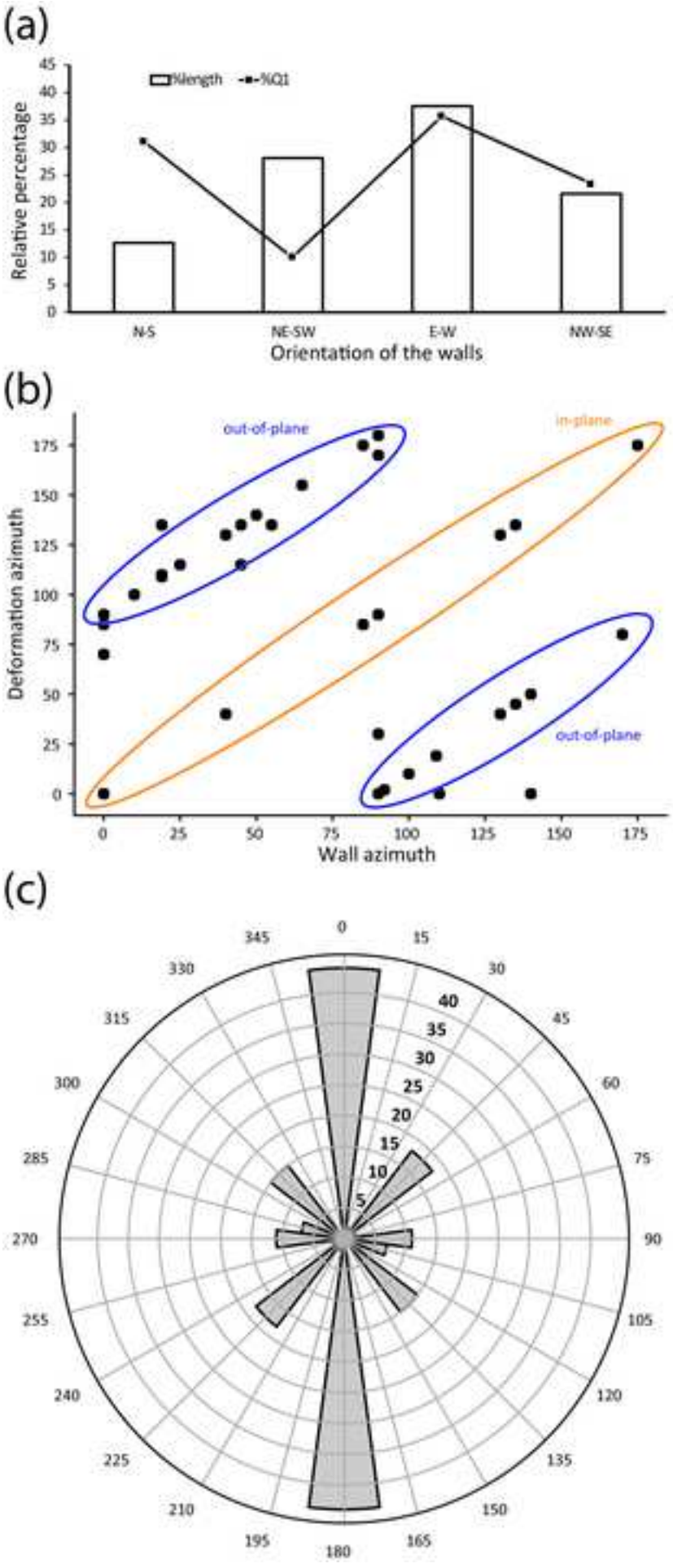

Figure 9

Click here to access/download;Figure;Fig9_crop.tif

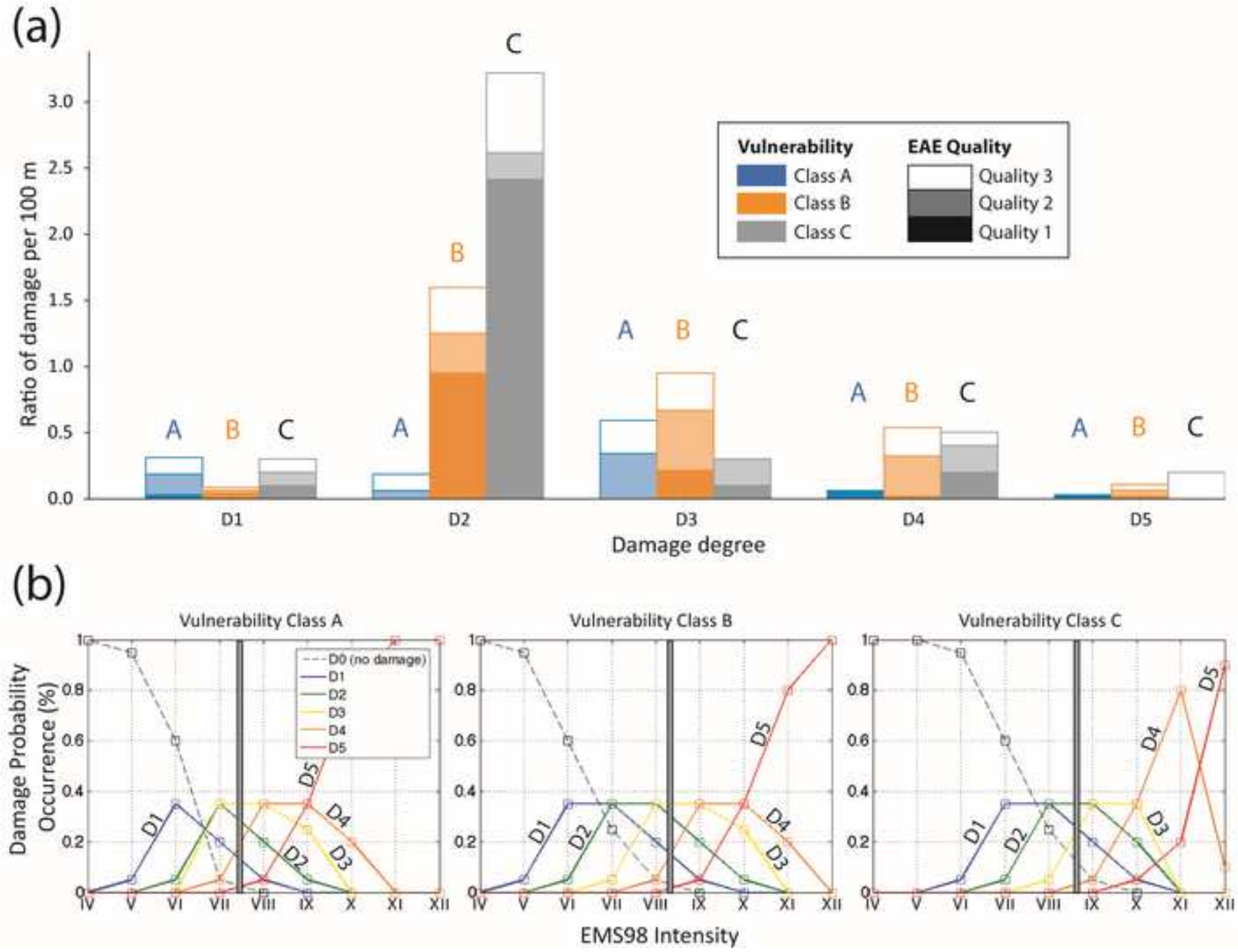

Figure 10

Click here to access/download;Figure;Fig10_300.tif

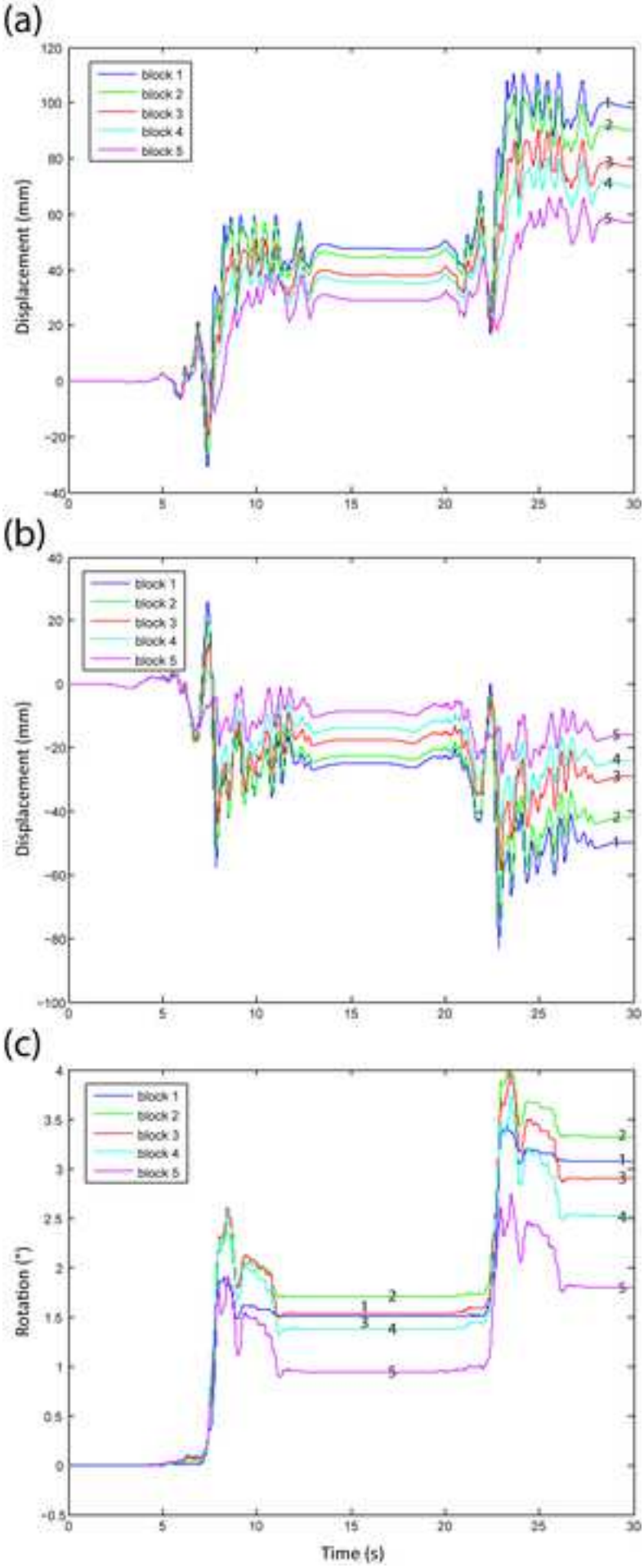

Historical earthquake scenarios for the middle strand of the North Anatolian Fault deduced from archeo-damage inventory and building deformation modeling

Yacine Benjelloun, Julia de Sigoyer, Hélène Dessales, Laurent Baillet, Philippe Guéguen, Mustafa Sahin

Supplemental Material

Table S1: Catalogue of earthquakes with effects in Iznik and neighbouring areas. Ms=surface wave magnitude. For the magnitude and epicentre location, we provide the different ranges found among the references.

Table S2: Description of the damage EAE observed in Iznik area.

Table S3: Description of the repair EAE observed in Iznik area.

Table S4: Length of walls and EAE of different qualities for each wall orientation range. The percentages in length and EAE were computed on the total wall length and total number of EAE in each quality class respectively.

Table S5: Characteristics of the earthquake used for the simulations on the obelisk.

Figure S1: Summary of the construction history of Iznik walls, after Schneider and Karnapp (1938) and Foss and Winfield (1986). After the construction of the walls in the 3rd century AD, the successive interventions and restoration works are drawn in color. The state of the walls preceding each intervention is drawn in grey.

Figure S2: (a) Drawing of Iznik obelisk with the dimensions and arrangement of the different blocks as measured on the field. The western face is given as an example on the left. (b) 3D mesh of the obelisk used for numerical modeling. (c, d) First and second main vibration modes for eigen frequencies of 7.8 and 7.84 Hz respectively. The initial shape of the obelisk is drawn in black, and the distribution of motion in color.

Table S1

Click here to access/download;Supplemental Material (Main Page, Tables, and Figures);TableS1.xlsx

Date AD	Affected localities	Effects in Nicaea/Iznik	Estimated Ms	
29-32	Bithynia, Nicaea	Most houses destroyed, tax exemptions for damaged cities in Asia Minor and imperial donations for repairs	6-7	
121	Bithynia, Nicomedia, Nicaea, probably Aoria	Great part of the city destroyed, publicly funded reconstruction, rebuilding of the fortifications	7.4, 7+	
358	Bithynia, Nicomedia, Nicaea, Perinthus, Constantinople	Destruction ? (severity unknown)	7.4, 7+	
362	Nicomedia, Nicaea, Constantinople	"a good part of the city was destroyed"	6-7, 6.8+	
368	Bithynia, Nicaea	Complete destruction, "sea wave" (one source)	6-7, 6.8	
478	Bithynia, Nicomedia, Helenoupolis, Constantinople, Nicaea	Damage ?, sea/lake wave	7.3, 7+	
554	Constantinople, Nicomedia, Nicaea	Partly damaged ? (one source only)	7, 6-7	
740	Eastern part of Marmara, Bithynia, Nicomedia, Praenetos (Karamursel), Nicaea, Constantinople	Complete destruction, "a single church survived"	7.1, 7+	
1065	Nicaea	Almost complete destruction, Widespread damage on churches, the city walls and numerous houses		6.8
2 Sep 1754	Izmit, Istanbul, Geyve, Bursa, Izmir (felt)	A few houses ruined, no casualties	7, 7+	
17 Sep 1857	Gemlik, Yalova, Bursa, Iznik (felt), Izmit (felt), Istanbul (felt)	Felt	5-6	
7 June 1860	Bursa, Istanbul (felt)	Panic, collapse of a few walls, no serious damage	5-6	
Nov 1860	Prusa (felt), Iznik (felt)	Several shocks occurring over a month	<5?	
19 Apr 1878	Lake Sapança, Izmit, Labinia, Esme, Adapazari, Akyazi, Bursa, Geyve, Iznik, Istanbul (felt)	Slight damage	5.5-6.1	
3 March 1893	Iznik, Yenisehir (felt), Istanbul (felt)	Slight damage on a few buildings	<5?	

10 Jul 1894	Adapazari, Istanbul, Sapanca, Izmit, Karamursel, Hersek, Yalova, Karaköy, Katirli, Gemlik, Mudanya, Iznik, Pendik, Bandirma, Bursa	Damage? (lack of details)	7.3

References

1=Ambraseys (2002)
2=Ambraseys (2009)
3=Guidoboni et al. (1994)
4=Ambraseys and Finkel (1991)
5=Ambraseys (2000)
6=Ambraseys and Jackson (1998)

Lat	Lon	Quality of epicenter location	NAF strand involved
40.5	30.4-30.5	poorly constrained	Middle (close to NAF junction?)
40.5	30.1	well constrained	Middle
40.7	30.2	well constrained	North
40.7	29.8-30.2	well constrained	North
40.5	29.5-30.5	well constrained	Middle
40.7	29.8	very well constrained	North
40.7-40.8	29.5-29.8	well constrained	North
40.7	27.7-29.6	well constrained	North
40.4	30	not given	Middle
40.7-40.8	29-30.1	poorly constrained	North
40.4	29.2	well constrained	Middle
40.3	29.3	not given	South?
		not given	unknown
40.7	30.2	not given	North
		not given	Middle?

40.7	27.5-29.6	very well constrained	North

Sources	References
Phlegon (Olympiads, 2nd c. AD), Eusebius (Hist, 2-3rd c. AD), Hieron. (Hist, 4-5th c. AD), Orosius (early fifth century)	1, 2, 3
Eusebius (Hist, 2-3rd c. AD), Hieron. (Hist, 4-5th c. AD)	1, 2, 3, 4
Sozomen (5th c. AD)	1, 2, 3
Ammianus Marcellinus (4th c. AD), John of Nikiu (7th c.)	1, 2, 4
Idatius (Cons. Const., 5th c. AD), Socrates Scholasticus (5th c), Hieron. (Hist., 4-5th c. AD), John of Nikiu (7th c) and others	1, 2, 3, 4
One late source	1, 2, 3
Vit. Sym. Iun (6th-7th c AD)	1, 2, 3, 6
Theophanes (8-9th), Michael Syrianus	1, 2, 3, 4
Attaliates (11th), Scylitzes (from public records?)	1,2
BC Misc. PD (contemporaneous)	1, 2, 4
Perrey (1860)	2
Perrey (1862c, 1875a), Schmiddt (1879)	2
Perrey (1862c)	2
Schmidt (1879)	1, 2, 4, 5
Rebeur-Paschwitz (1895)	2

contemporaneous	1, 2

Table S2

Click here to access/download;Supplemental Material (Main Page, Tables, and Figures);TableS2.xlsx

Damage EAE dataset

EAE ID	N	E	Location
AQ1	40.428672	29.729736	Arch N face
AQ2	40.428716	29.729896	Arch N face
AQ3	40.428716	29.730155	Wall N face
AQ5	40.428731	29.730457	Arch N face
AQ6	40.428781	29.730702	Wall N face
AQ7	40.428773	29.730776	Wall N face
AQ8	40.428767	29.730858	Wall N face
AQ9	40.428764	29.730921	Wall N face
AQ48	40.428764	29.730921	Arch N face
AQ10	40.428788	29.731086	Wall N face
AQ11	40.428739	29.731444	Wall N face
AQ12	40.42874	29.731493	Wall N face
AQ13	40.428713	29.731968	Wall N face
AQ14	40.428737	29.731699	Wall N face
AQ16	40.428705	29.732405	Wall N face
AQ17	40.428555	29.7356	Wall N face
AQ18	40.428524	29.736018	Wall N face
AQ19	40.428779	29.730635	Wall S face
AQ20	40.428719	29.730503	Wall S face
AQ22	40.428662	29.72996	Wall S face
AQ25	40.4286833	29.7302505	Wall S face
AQ28	40.42872	29.730365	Wall N face
AQ33	40.428713	29.730347	Wall N face
AQ34	40.428717	29.73037	Wall N face
AQ37	40.428742	29.73052	Wall N face
AQ38	40.428746	29.730554	Wall N face
AQ44	40.428405	29.736874	Reinforcement brick structure
AQ45	40.428655	29.729618	Arch
AQ46	40.4269	29.7388	Underground section
AQ47	40.4233	29.7418	Underground section
W1	40.4296	29.728884	Outer wall 45/46, outer facing
W2	40.429676	29.728791	Outer wall, outer facing
W3	40.429913	29.728396	Inner wall, T46 base
W4	40.429913	29.728396	Inner wall, T46 base
W5	40.429913	29.728396	Inner wall, T46 base
W6	40.429913	29.728396	Inner wall, T46 base
W7	40.429913	29.728396	Inner wall, T46 base
W8	40.429913	29.728396	Inner wall, T46 base
W9	40.429913	29.728396	Inner wall, T46
W10	40.430041	29.728097	W46-47
W11	40.431735	29.726386	Isolated ashlar wall section
W12	40.431735	29.726386	Isolated ashlar wall section
W13	40.431735	29.726386	Isolated ashlar wall section
W15	40.431735	29.726386	Isolated ashlar wall section

W16	40.431735	29.726386	Isolated ashlar wall section
W17	40.432509	29.725585	W52/53
W18	40.432822	29.725154	T53 base
W19	40.432822	29.725154	T53 base
W20	40.433132	29.724737	T54
W21	40.432959	29.724893	W53/54
W22	40.432959	29.724893	W53/54
W23	40.432959	29.724893	W53/54
W24	40.433132	29.724737	T54 base
W26	40.433321	29.724417	W54/55 inner wall
W27	40.433324	29.724601	W54/55 outer wall
W28	40.433731	29.724092	W55/56 outer wall
W29	40.433686	29.723945	W55/56 inner wall
W30	40.434126	29.723269	T57
W31	40.434126	29.723269	T57 base
W32	40.434126	29.723269	T57 base
W33	40.434126	29.723269	T57 base
W34	40.434126	29.723269	T57 base
W36	40.434126	29.723269	T57 base
W37	40.434126	29.723269	T57 base
W38	40.434126	29.723269	T57 base
W39	40.434126	29.723269	T57 base
W40	40.434126	29.723269	T57 base
W41	40.434402	29.722751	T58 eastern part
W42	40.434402	29.722751	T58 central part
W43	40.434402	29.722751	T58 eastern western part
W44	40.435115	29.722236	W59/60
W46	40.435342	29.721959	T61
W48	40.435383	29.722171	Outer wall in front of T61
W50	40.435628	29.721456	W62/63
W51	40.435894	29.721191	W63/64
W52	40.436003	29.721319	Outer wall in front of T64
W53	40.436131	29.721105	W64/65
W55	40.436225	29.721108	W64/65 and T65
W56	40.436454	29.72052	Istanbul Gate, inner door
W57	40.436427	29.720472	Istanbul Gate, inner door, inner facing
W58	40.436477	29.720354	Istanbul Gate, inner door, outer facing
W59	40.436448	29.720308	Istanbul Gate, inner door
W60	40.43647	29.720394	Istanbul Gate, inner door, outer facing
W61	40.436576	29.720927	T66
W62	40.436576	29.720927	T66
W63	40.436576	29.720927	T66
W64	40.436447	29.720995	W65/66
W65	40.436742	29.720384	Istanbul Gate, outer wall, west tower
W66	40.436742	29.720384	T68
W67	40.436506	29.720047	W68/69 outer facing
W68	40.436235	29.719516	W69/70 outer wall

W69	40.436235	29.719516	W69/70 inner wall, outer facing
W71	40.436235	29.719516	W69/70 inner wall, outer facing
W72	40.436235	29.719516	W69/70 inner wall, outer facing
W195	40.436027	29.71912	T70
W74	40.436042	29.718953	W70/71 outer wall, inner facing
W75	40.435916	29.718792	W70/71 outer wall, inner facing
W76	40.435916	29.718792	W70/71 outer wall, inner facing
W77	40.436042	29.718953	W70/71 outer wall, inner facing
W78	40.43568	29.718494	T71
W79	40.43568	29.718494	T71
W80	40.43568	29.718494	T71
W82	40.435075	29.717725	W72/73 inner wall
W83	40.434984	29.717525	W72/73 inner wall
W84	40.434931	29.717425	T73
W85	40.434811	29.717285	W73/74
W87	40.434563	29.71684	T74
W88	40.434563	29.71684	T74
W89	40.434494	29.716566	W74/75 outer wall
W91	40.432208	29.71437	W80/84
W92	40.429951	29.713724	T84
W94	40.427988	29.713183	T88
W95	40.427319	29.712449	W98/lake
W97	40.426883	29.713197	T90
W98	40.425862	29.71382	T92
W99	40.425793	29.713872	South Lake Gate, N side, inner face
W100	40.425793	29.713872	South Lake Gate, N side, inner face
W102	40.425567	29.713889	T94
W192	40.425567	29.713889	W94/95
W103	40.425567	29.713889	W94/95
W104	40.425567	29.713889	W94/95
W105	40.425567	29.713889	W94/95
W107	40.423719	29.716242	Corner of outer wall in front of T104
W108	40.423556	29.716381	W104/105
W109	40.423151	29.716195	W105/106 outer wall, outer facing
W110	40.422964	29.716464	T106
W111	40.422805	29.71671	T107
W112	40.422977	29.718715	T113
W113	40.42347	29.719166	Yenisehir central Gate, inner facing
W114	40.42347	29.719166	Yenisehir central Gate, inner facing
W115	40.42347	29.719166	Yenisehir central Gate, inner facing
W116	40.423557	29.719208	Yenisehir inner Gate
W117	40.423458	29.719218	Yenisehir central Gate, inner facing
W118	40.423436	29.719221	Yenisehir central Gate
W119	40.423419	29.719221	Yenisehir central Gate, outer facing
W120	40.423419	29.719221	Yenisehir central Gate, inner facing
W121	40.423256	29.719346	Outer wall in front of T1
W122	40.423256	29.719346	Outer wall in front of T1

W190	40.423256	29.719346	T1
W191	40.423256	29.719346	T1
W183	40.423324	29.719195	Yenisehir outer Gate
W123	40.423444	29.720843	W4/5, inner wall, inner facing
W124	40.423412	29.720966	W5/6, inner wall, inner facing
W125	40.423396	29.721499	W6/7, inner wall, inner facing
W126	40.423397	29.720636	T4
W127	40.423384	29.720794	W4/5, inner wall, outer facing
W128	40.423376	29.720968	T5
W130	40.423355	29.721288	T6
W131	40.423355	29.72157	T7 west corner
W132	40.423324	29.722092	W8/9
W133	40.423324	29.722092	W8/9
W134	40.423291	29.722828	W10/11
W135	40.423267	29.722987	T113
W136	40.423121	29.724184	T15
W137	40.423122	29.724185	T15
W138	40.423163	29.724557	T16
W139	40.423164	29.724558	T16
W140	40.423147	29.72488	T17
W141	40.423148	29.724881	T17
W142	40.423109	29.725546	T19
W143	40.42311	29.725547	T19
W192	40.42311	29.725547	W19/20
W144	40.423073	29.725906	T20
W145	40.423122	29.725974	T20
W146	40.423285	29.725959	W20/21
W147	40.42366	29.726168	W21/22
W148	40.423768	29.726252	W22/23
W196	40.424062	29.726438	T23
W150	40.424114	29.726442	W23/24
W151	40.424634	29.726782	T26
W152	40.424528	29.726733	W25/26
W153	40.424529	29.726734	W25/26
W158	40.424693	29.726793	W26/27
W159	40.425094	29.726994	W27/28
W160	40.425358	29.727153	W28/29
W162	40.428028	29.728775	T39
W163	40.428029	29.728776	T39
W164	40.427785	29.728624	T38
W165	40.427786	29.728625	T38
W166	40.427334	29.728366	T37
W168	40.426912	29.728086	T35
W194	40.426912	29.728086	T35
W193	40.426421	29.727916	T33
W170	40.427809	29.728558	T38, inner face
W171	40.42646	29.727753	T33, inner face

W172	40.426255	29.727625	T32, inner face
W173	40.425552	29.727225	T29, inner face
W175	40.425552	29.727225	W26/27, inner face
W176	40.425552	29.727225	W26/27, inner face
W177	40.424649	29.726709	T26, inner face
W178	40.424649	29.726709	W26/25, inner face
W180	40.423714	29.726154	T21, inner face
W181	40.423212	29.724522	T16, inner face
W182	40.423212	29.724522	T16, inner face
W184	40.436644	29.720502	Istanbul central Gate
W185	40.428902	29.729214	Lefke central Gate
W186	40.42885	29.729057	Lefke Gate western area
W187	40.42885	29.729057	Lefke Gate western area
W188	40.428959	29.729073	Lefke Gate western area
W189	40.428959	29.729073	Lefke Gate western area
C1	40.429817	29.726843	Yesilcamii, west wall
C2	40.429817	29.726843	Yesilcamii, west wall
C4	40.429861	29.726921	Yesilcamii, north wall
C5	40.429861	29.726921	Yesilcamii, north wall
C48	40.429861	29.726921	Yesilcamii, north wall
C6	40.428146	29.719755	Celebi Camii, north wall
C8	40.428146	29.719755	Celebi Camii, north wall
C9	40.428306	29.720615	II. Murhat Hamami, east wall
C10	40.42822	29.720528	II. Murhat Hamami, south wall
C11	40.429246	29.720232	Aya Sofya, north wall, inner facing
C12	40.429253	29.720228	Aya Sofya, NE room
C15	40.429213	29.720259	Aya Sofya, NE wall of nave
C17	40.429253	29.720228	Aya Sofya, NE room
C48	40.426283	29.717399	Terracotta building next to theater
C18	40.42645	29.716512	Theater, southern side
C19	40.42652	29.716529	Theater, entry corridor
C21	40.426367	29.71674	Theater, corridor wall
C23	40.426624	29.716357	Theater, western side
C24	40.426624	29.716357	Theater, western side
C25	40.426468	29.717228	Theater, SE side
C28	40.426468	29.717228	Theater, S corridor
C29	40.426786	29.716731	Theater scene, outer western vault
C32	40.426786	29.716731	Theater scene, inner western vault
C33	40.426774	29.717086	Theater scene, inner eastern vault
C35	40.426449	29.7169	Theater, inner corridor
C36	40.426463	29.716554	Theater, S side
C37	40.426794	29.717116	Theater, NE side
C39	40.426866	29.716992	Theater, NE side
C40	40.428964	29.731713	Candarli Hayretin Pasa, east room
C41	40.428964	29.731713	Candarli Hayretin Pasa, east room
C42	40.428964	29.731713	Candarli Hayretin Pasa, east room
C46	40.428969	29.731616	Candarli Hayretin Pasa, west room

C47	40.428969	29.731616	Candarli Hayretin Pasa, west room
O1	40.487589	29.701961	Obelisk
B1	40.42575	29.7095	Lake basilica

EAE description	Wall azimuth	Deformation azimuth
Important sinter deposit	90	
Collapsed facing	90	0
Collapsed facing	90	0
Sinter deposit	90	
Sinter deposit	90	
Collapse facing	90	
Large and deep collapse	90	0
Sinter deposit and collapse	90	0
Collapsed facing	90	0
Large and deep collapse	90	0
Collapsed facing + sinter deposit	90	0
Thick sinter deposit	90	
General wall warping northward	90	0
Thick sinter deposit	90	
Collapsed facing	90	0
Wall warping southward	90	0
Wall warping northward	90	0
Sinter deposit	90	
Tilted wall	90	0
Sinter deposit	90	
Sinter deposit	90	
Sinter deposit	90	
Top of wall warping northward	90	0
Tilted wall	90	0
Tilted wall	90	0
General wall warping northward	90	0
Destruction of top of structure	90	
Damaged keystone	90	
Vertical offset		
Vertical offset		
Collapsed part between cracks	135	
Significant crack at junction between tower and wall	135	
Expulsion of block corners, cracks	0	70
In-plane offset blocks	0	0
In-plane offset blocks	135	135
Out-of-plane offset blocks	135	45
In-plane offset blocks	135	135
Out-of-plane offset blocks	135	45
Cracks in terracotta masonry	135	
Expulsed block corners	135	
Anticlockwise block rotation + apparent offset	100	10
In-plane offset blocks	90	90
Dropped ashalrs	90	
Anticlockwise block rotation	88	

Out-of-plane offset adjacent blocks	92	2
Expulsed block corners + out-of-plane shift	130	40
Expulsed block corners	130	
Expulsed block corner + in-plane offset	40	40
Facing collapse + cracks in core		
Out-of-plane block shift	130	40
Cracks in block	130	
Expulsed block corners	130	
Lower part of tower base is shifted outward	130	40
Significant crack with no vertical offset	130	
Crack	130	
Collapsed arch keystone	120	
Significant crack with no vertical offset	130	
Cracks	130	
In-plane offset blocks	40	40
In-plane offset blocks	40	40
In-plane offset blocks	130	130
Out-of-plane offset blocks	130	40
In-plane offset blocks	130	130
In-plane offset blocks	130	130
Out-of-plane offset blocks	130	40
In-plane offset blocks	40	40
Out-of-plane offset blocks	40	130
Cracks and structural collapse		
Multiple cracks		
Crack and facing collapse		
Tilted ashlar	0	90
Destruction of superstructure		
Sinistral offset of wall	130	40
Significant crack and lower facing collapse	140	
Expulsed block corner + crack	170	
Out-of-plane arch distorsion	170	80
Expulsed block corners	170	
Significant structural collapse		
Out-of-plane block shift	90	180
Out-of-plane shift + tilting	90	180
Anticlockwise block rotation	90	
Column collapse	90	30
Out-of-plane ashlar shift and rotation	90	0
General tilting	140	0
Facing collapse under window	140	50
Facing collapse under window	50	140
Superstructure collapse	140	50
Vault collapse		
Facing collapse	0	85
Cracks + collapse	53	
Wall offset	55	

Clockwise block rotation	55	
Significant crack + tilted masonry	55	
Superstructure collapse	55	135
Slight damage on blocks	55	
Partial out-of-plane facing expulsion	45	135
Offset and tilted arch	50	140
Oblique parallele cracks	45	
Tilted wall	45	135
Slightly expusled angle	135	135
Partial collapse		
Collapsed blocks	135	45
Total destruction	45	135
Superstructure collapse	45	135
Facing collapse	45	115
Crack visible from both sides of wall	45	
Crack	45	
Collapse of western angle	135	45
Collapsed keystones on two successive arches	50	
Widespread destruction		
Parallel cracks		
Small crack initiated at window	10	
Apparent wall offsets	90	
Crack initiated at window	150	
Crack through beam holes		
Anticlockwise block rotation + expulsed block corner	0	
Block shifts + cracks	90	90
Expulsed block corner	0	
Expulsed block corner	90	
Block rotations	90	
Warped masonry + offset	90	0
Ashlar phase tilted southward + warping	90	0
Outward corner expulsion		
Collapsed blocks		
Facing collapse	0	90
Destruction of eastern part + cracks at window		
Partial destruction of superstructure		
Partial collapse around window	65	155
Collapsed blocks	90	0
Block expulsion	90	
Clockwise block rotation	90	
Block shift + rotation	96	
Shifted arch keystone	90	0
Shifted arch keystone	90	0
Damaged keystone	90	
Expulsed block corners	90	
Dropped central arch	90	
Southward tilting	90	170

Collapsed facing under window	0	
Collapsed facing at window	0	
Damaged keystones	90	
Large vertical crack	90	
Large vertical crack with offset layers	90	
Two "conjugated cracks" crossing arch	90	
Large structural collapse	90	0
Cracks and facing collapse	90	0
Expulsed block corner	0	
Sub-horizontal crack at base	135	
Anti-clockwise block rotation	90	
Cracks	90	
Facing collapse	90	0
Partial collapse	90	0
Total destruction		
Partial destruction of superstructure	0	90
Out-of-plane shift + tilting	110	0
Crack	0	
Crack	0	
Crack at base	0	
Crack	0	
Out-of-plane shift of window frame	90	0
Large crack with general shift of superstructure		45
Collapse of superstructure	90	0
Large vertical fissure		
Large vertical fissure + expulsion of upper fragment	10	100
Clockwise block rotation	19	
Partial collapse	19	110
Block and facing collapse	19	110
Slight damage on superstructure		
Cracked ashlar	19	
Large facing collapse	19	
Anticlockwise block rotation	19	
Out-of-plane shift	19	109
Large facing collapse	19	109
Superstructure collapse	19	109
Block collapse	19	109
Large crack and outward tilting	109	19
Large crack + facing collapse	109	
Large vertical crack	109	
Large vertical crack	19	
Large collapse + tension crack in superstructure	109	
Destroyed facing		
Crack	109	
Crack and facing collapse		
Large vertical, penetrative crack	19	
Two cracks, slight deformation of masonry	19	

Two vertical cracks	19	
Vertical crack	19	
Cracked and slightly dislodged block + facing collapse	19	
Cracked and shifted ashlar	19	135
Damaged arch + facing collapse	19	
Vertical crack, penetrative through masonry and base ashlar	19	
Left-lateral wall offset + slight wall warping	19	
Right-lateral offset of upper facing	90	0
Damaged arch keystone	90	
Shifted voussoir	90	
Large cracks and damaged voussoirs	0	
Lintel shift	0	0
Collapsed block	90	0
Shifted block	0	0
Shifted blocks	90	90
Dropped keystone	175	
In-plane offset blocks	175	175
Dropped and shifted keystones	85	175
In-plane offset blocks	85	85
Damaged voussoirs	85	
Shifted block	85	175
Cracked column capital		
Damaged voussoirs	175	
Damaged voussoirs	85	
Clockwise block rotation		
Deformed pavement		
Dislodged blocks	90	
Partial collapse of vaults	90	
Collapsed keystones	2	
Collapsed block	130	40
Dropped vault block		
Multiple cracks in block		
Expulsed block corners		
Out-of-plane block shift	0	90
Shifted keystone and voussoirs	25	115
Dropped vault block		
Shifted keystone and voussoirs	0	90
Cracked keystone	0	
Out-of-plane block shift	0	90
Dropped vault block		
Destroyed arch	90	
Collapsed block	90	0
Shifted stair block	90	0
Cracked gravestone	0	
Cracks + corner expulsion		
Horizontal crak of gravestone base		
Horizontal cracks	0	

Vertical crack + slight shift	90	0
Shifted and rotated blocks		
Destruction		

Deformation strike	Other measurement	Terminus post quem	Terminus ante quem
		1208	
0		527	
0		527	
		1097	
		1097	
		1097	
0		1097	
0		527	
		1097	
0		1097	
0		527	
		1097	
		1097	
		1097	
0		527	
		527	
		527	
		527	
180		527	
		527	
		527	
		1097	
		527	
	dip 80S	527	
		1097	
		1097	
		527	
		1208	
	offset >50 cm	527	
	offset >50 cm	527	
		1222	
		1222	
		3rd c.	1254
	offset 5.5 cm	3rd c.	1254
	offset 4-4.5 cm	3rd c.	1254
45	offset 5-9 cm	3rd c.	1254
	offset 2.5-3 cm	3rd c.	1254
45	offset 2.5 cm	3rd c.	1254
		3rd c.	1254
		3rd c.	
	rotation 10°; offset 8-10cm	3rd c.	
	offset 5-9 cm	3rd c.	
	drop 6 cm	3rd c.	
	rotation 4°	3rd c.	

	offset 3-4 cm each	3rd c.		
40	shift 3 cm	3rd c.		
		3rd c.		
		3rd c.		
			858	
40			730	
			730	
			730	
40			858	
			730	
			1222	
			1222	
		3rd c.		
		3rd c.		
	shift 2 cm	3rd c.		1097
	shift 4 cm	3rd c.		1097
	shift 15 cm and 4 cm	3rd c.		1097
40	shift 3.5 cm	3rd c.		1097
	shift 3 cm	3rd c.		
	shift 3-4 cm	3rd c.		
40	shift 4 cm; dip 5-10°	3rd c.		
	shift 2.5-3.5 cm	3rd c.		
310	shift 4 cm	3rd c.		
	crack plane N060 dip 70E		1260	
	crack plane N040 dip 60		1260	
	crack dip > 80E		1260	
90	dip 5°	3rd c.		
			1208	
	offset 15 cm		1222	
		3rd c.		
		3rd c.		
	keystone offset 6 cm		1222	
			858	
			858	
180	shift 5 cm	3rd c.		
180	shift 6 cm; tilt 5°	3rd c.		
	max rotation 20°	3rd c.		1185
30		3rd c.		
0		3rd c.		1185
0			858	
50			858	
140			858	
50			858	
			1222	
265			1208	
		3rd c.		
	dextral offset 10 cm		1222	

			1143	
		3rd c.		
315			1143	
			730	
135			1222	
	dextral offset 20 cm		1222	
	crack dip 45° NE		1222	
	dip 85° NW		1222	
315			730	
			730	
45			730	
315			730	
315			1143	
295		3rd c.		
	crack dip 70W	3rd c.		
	crack plane azimuth 165	3rd c.		
225		3rd c.		
			1222	
		3rd c.		
		3rd c.		1330
			1260	
	left-lateral offset 40 cm		730	
		3rd c.		
	crack plane 030 65W	3rd c.		
	rotation 6°	3rd c.		1254
	shifts 1-11cm	3rd c.		1254
			730	1254
			730	1254
			730	1254
			1208	
	tilt 10°		730	1254
			1222	
		3rd c.		
			1222	
			1208	
		3rd c.		
155			858	
0		2nd c.		
		2nd c.		
	rotation 8°	2nd c.		
	rotation 5°	2nd c.		
0	horizontal shift + slight drop	2nd c.		
180		2nd c.		
		2nd c.		
		2nd c.		
			1222	
170			1222	

			858	
			858	
			1222	
		3rd c.		
		3rd c.		
	crack plane 90, dip 60°		1208	
180		3rd c.		
180		3rd c.		
	shear plane NE-SW		858	
	plane azimuth NE-SW, dip 20N	3rd c.		
			1143	
	dip 35-40°	3rd c.		
180		3rd c.		
180			1222	
			858	
90			1208	
180	shift 6 cm; tilt 5°		858	1222
	dip 50 NW		1208	
	dip 45 S		1208	
	dip 55 S		858	
	dip 50 S		858	
180			1208	
			1208	
180			1065	
	dextral offset		1222	
100	dextral offset		1222	
			730	
110			730	
110			730	
			1222	
			730	
			1208	
			730	
109			730	
109			730	
109			730	
109			730	
19			858	
	crack dip 55 N		858	
	crack dip 70 S	3rd c.		
	crack dip 80 N	3rd c.		
	crack dip 70 N		1065	
		3rd c.		
	crack dip 60°	3rd c.		
			1065	
		3rd c.		1065
	crack dip 80°	3rd c.		1065

	crack dip 80°	3rd c.		858
	slight vertical shift in masonry	3rd c.		1065
		3rd c.		
135		3rd c.		
		3rd c.		
		3rd c.		858
	offset 30-40 cm	3rd c.		
		3rd c.		1065
		3rd c.		
		2nd c.		858
		2nd c.		
180		3rd c.		1254
180		3rd c.		858
0		3rd c.		
270		3rd c.		
			1378	
175			1378	
175			1378	
			1378	
			1378	
355			1442	
			1442	
			1421	
			1421	
	rotation 5°		527	787
			1260	
			527	787
			1260	
			1208	
220		2nd c.		
		2nd c.		
		2nd c.		
		2nd c.		
270		2nd c.		
	tilt 5-10°; vertical shift 2.5-5 cm	2nd c.		
		2nd c.		
90	tilt 6°; drop 1-2 cm	2nd c.		
		2nd c.		
270		2nd c.		
		2nd c.		
		2nd c.		
0		2nd c.		
0		2nd c.		
			1387	
			1387	
			1387	
			1387	

left-lateral 1387

1st c

Vulnerability class	Damage grade	Non-seismic causing processes?	Quality rank	Ref (if other study)
B	3	Recent, natural decay	3	Benjelloun et al. (2018)
B	3	Recent, natural decay	3	Benjelloun et al. (2018)
A	3	War damage	2	Benjelloun et al. (2018)
A	2	Recent, natural decay	3	Benjelloun et al. (2018)
A	2	Recent, natural decay	3	Benjelloun et al. (2018)
A	3	War damage	2	Benjelloun et al. (2018)
A	3	War damage	2	Benjelloun et al. (2018)
A	3	War damage	2	Benjelloun et al. (2018)
A	3	War damage	2	Benjelloun et al. (2018)
A	3	War damage	2	Benjelloun et al. (2018)
A	3	Recent, natural decay	3	Benjelloun et al. (2018)
A	3	Recent, natural decay	3	Benjelloun et al. (2018)
A	1	Soil instability, original construction	3	Benjelloun et al. (2018)
A	2	Recent, natural decay	3	Benjelloun et al. (2018)
A	3	Man-made damage, natural decay	3	Benjelloun et al. (2018)
A	1	Original construction	3	Benjelloun et al. (2018)
A	1	Original construction	3	Benjelloun et al. (2018)
A	2	Recent, natural decay	3	Benjelloun et al. (2018)
A	1	Soil instability	2	Benjelloun et al. (2018)
A	3	Recent, natural decay	3	Benjelloun et al. (2018)
B	2	Recent, natural decay	3	Benjelloun et al. (2018)
A	3	Recent, natural decay	3	Benjelloun et al. (2018)
A	1		1	Benjelloun et al. (2018)
A	1	Soil instability	2	Benjelloun et al. (2018)
A	1	Soil instability	2	Benjelloun et al. (2018)
A	1	Original construction	2	Benjelloun et al. (2018)
B	4	Man-made damage	3	Benjelloun et al. (2018)
B	2	Recent, vehicles traffic	3	Benjelloun et al. (2018)
B	1		1	Benjelloun et al. (2018)
B	1		1	Benjelloun et al. (2018)
A	3	Original construction, natural decay	3	
A	3	Foundation failure, soil instability	3	
B	2		1	
B	2		1	
B	2		1	
B	2		1	
B	2		1	
B	2		1	
B	3		1	
B	2		1	
C	2	Dubious context, man-made	3	
C	2	Dubious context, man-made	3	
C	2	Dubious context, man-made	3	
C	2	Dubious context, man-made	3	

C	2	Dubious context, man-made	3
B	2		1
B	2		1
B	2		1
B	4	War damage	2
B	2		1
B	2	War damage	2
B	2		1
B	2	Original construction	2
B	3		1
B	3		1
B	3	Man-made damage	2
B	3		1
B	2	War damage	2
B	2		1
B	2		1
B	2		1
B	2		1
B	2		1
B	2		1
B	2		1
B	2		1
B	2		1
B	4	Natural decay	2
B	2	Natural decay	2
B	4	Natural decay	2
B	2		1
B	5	War damage	2
A	1	Original construction	3
B	4	War damage	2
B	2		1
A	3	Vegetation	2
B	2		1
B	3	War damage	2
C	2		1
C	2		1
C	2		1
C	5	Dubious context, natural decay	3
C	2		1
B	2	Foundation failure, soil instability	3
B	3	War damage	2
B	3	War damage	2
B	5	War damage	2
A	4		1
B	4	Natural decay	2
B	3	War damage, natural decay	3
B	2	Original construction	3

B	2		1
B	3	War damage	2
B	3	War damage	2
C	1	War damage, natural decay	3
A	3	Original construction	2
A	3	Foundation failure, soil instability	3
A	2	Natural decay	2
A	1	Soil instability	2
C	2		1
C	4	War damage, natural decay	3
C	2	War damage	2
C	5	War damage, natural decay	3
B	4	War damage, natural decay	3
B	4	War damage, natural decay	3
B	3	War damage	2
B	3	War damage	2
B	4	War damage, natural decay	3
A	4		1
B	5	Dubious context	3
B	4	Natural decay	2
B	2	Natural decay	2
C	2	Original construction	3
B	2	War damage, natural decay	3
B	2	War damage, natural decay	3
B	2		1
B	2		1
C	2		1
C	2		1
C	2		1
B	1	Original construction	2
C	1		1
A	3	Natural decay	2
B	2	War damage, natural decay	3
A	5		1
B	4	Natural decay	2
B	4	Natural decay	2
B	3	War damage, natural decay	3
C	4	War damage	2
C	4		1
C	2		1
C	2		1
C	2		1
C	2		1
C	4		1
C	2		1
A	3	Soil instability	2
A	2	Soil instability	2

B	4	War damage	2
B	4	War damage	2
A	3	Natural decay	2
B	3	War damage	2
B	3	Original construction	3
B	3	Natural decay	2
B	4	War damage, natural decay	3
B	4	War damage, natural decay	3
B	2		1
B	3	War damage	2
B	2		1
B	3	War damage	2
B	4	War damage, natural decay	3
B	4	Natural decay	2
B	5	Dubious context	3
B	4	Natural decay	2
B	2		1
B	3	Natural decay	2
B	3	Natural decay	2
C	3	War damage	2
C	3	Natural decay	2
B	2		1
B	4		1
B	4	War damage	2
B	3		1
B	3		1
B	2	War damage	2
B	3	War damage, natural decay	3
B	4	War damage	2
C	1	Natural decay	2
B	2	War damage	2
B	4	Dubious context	3
B	2	War damage	2
B	2	War damage	2
B	2	War damage, natural decay	3
B	2	War damage, natural decay	3
B	2	War damage	2
B	3	Natural decay, war damage	3
B	3	War damage	2
B	3	War damage, natural decay	3
B	3	War damage, natural decay	3
B	4	War damage, natural decay	3
B	4	War damage, natural decay	3
B	3	War damage, natural decay	3
B	3	War damage, natural decay	3
B	3		1
B	2	Natural decay	2

B	3		1
B	3		1
B	2		1
B	2		1
B	3	Natural decay	2
B	3		1
B	1	Original construction	3
B	2	Dubious context	3
B	3	Natural decay	2
C	2		1
C	2		1
C	4	Natural decay	2
C	3		1
C	2		1
C	2		1
C	2		1
C	2		1
C	2		1
C	2		1
C	2		1
C	2		1
C	2	Natural decay	2
B	2		1
B	2		1
B	2		1
B	2	Soil instability	2
B	2		1
B	3	Natural decay	2
B	3	Natural decay	2
B	3	Man-made	2
B	2	Natural decay, original construction	3
B	2	Natural decay	2
B	2		1
B	2		1
B	2		1
B	2	Natural decay, original construction	3
B	2		1
B	2		1
B	2		1
B	2	Natural decay, original construction	3
B	3	Man-made	2
B	2	Man-made	2
B	2		1
B	2	Dubious context	3
B	2	Dubious context	3
B	3	Dubious context	3
B	3	Dubious context	3

B	2	Dubious context	3
C	2		1
B	5		1

Table S3

Click here to access/download;Supplemental Material (Main Page, Tables, and Figures);TableS3.xlsx

Reconstruction EAE dataset

EAE ID	N	E	Location	Type
RC1	40.426492	29.716886	Theater, inner corridor	Reinforcement
RC2	40.429246	29.720232	Aya Sofya, N inner wall	Repair
RC3	40.429213	29.720259	Aya Sofya, NE wall of nave	Repair
RC4	40.429213	29.720259	Aya Sofya, N wall	Reinforcement
RC5	40.428306	29.720615	II. Murhat Hamami, east door	Reinforcement
RC8	40.42822	29.720528	II. Murhat Hamami, south door	Reinforcement
RC11	40.429817	29.726843	Yesilcamii, nort door	Reinforcement
RW2	40.42885	29.729057	Lefke Gate, SW area	Reinforcement
RW5	40.429913	29.728396	T46	Repair
RW6	40.434126	29.723269	T57 base	Repair
RW7	40.436477	29.720354	Istanbul inner Gate	Reconstruction
RW8	40.436235	29.719516	Outer wall in front of T61, inner facing	Repair
RW10	40.429951	29.713724	T84	Reconstruction
RW11	40.428476	29.713401	W87/88	Reinforcement
RW12	40.425793	29.713872	South Lake Gate	Reconstruction
RW13	40.425554	28.714165	W94/95	Reconstruction
RW14	40.425462	29.715602	T97	Reinforcement
RW18	40.423714	29.726154	T21, inner wall, inner facing	Repair
RW19	40.423212	29.724522	T16, inner wall, inner facing	Reconstruction
RAQ1	40.428735	29.730474	Close to arch 8, northern facing	Reconstruction
RAQ3	40.428728	29.731783	Aqueduct, northern facing	Reinforcement
RAQ4	40.42871	29.732231	Aqueduct, northern facing	Reconstruction
RAQ5	40.428702	29.732815	Aqueduct, northern facing	Reinforcement
RAQ7	40.4287	29.732951	Aqueduct, northern facing	Reinforcement
RAQ8	40.428403	29.736874	Aqueduct, northern facing	Reinforcement
RAQ9	40.428667	29.729747	Arch 7, southern facing	Reinforcement

Description	Date range	Ref (if other study)
Imbricated, polygonal bocks	2nd c.	
Pink mortar sealing	8th c.	
Terracotta and white mortar sealing	8th c.	
Walled windows	13th c. ?	
Seismoresistant technique on arch	Early 15th c.	
Seismoresistant technique on arch	Early 15th c.	
Seismoresistant technique on arch	Late 14th c.	
Walled opening	12-13th c.	
Light pink mortar on crack	12-13th c.	
Thicker terracotta masonry	12-13th c.	
Mixed terracotta+rubble masonry	1143-1180	
Bright mortar on wall offset	Early 13th c.	
Mixed terracotta+rubble masonry	Late 13th c.	
Buttress	Late 12th c.	
Terracotta masonry with yellowish pink mortar	Early 13th c.?	
Mixed terracotta+rubble masonry	12-13th c.	
Mixed terracotta+rubble masonry	1222-1330	
Mortar on wall offset		
Very similar style to surrounding walls		
Limestone and travertine rubble + marble spoils	Early 11th c.	Benjelloun et al. (2018)
Walled arch	6th-11th c.	Benjelloun et al. (2018)
Mixed materials (terracottas, spoils)	11th c.	Benjelloun et al. (2018)
Walled arch	6th-11th c.	Benjelloun et al. (2018)
Walled arch	6th-11th c.	Benjelloun et al. (2018)
Buttress-like brick structure	6th-11th c.	Benjelloun et al. (2018)
New travertine facing over terracotta	6th-11th c.	Benjelloun et al. (2018)

Table S4

Orientation	Length (m)	% Length	Q1	%Q1	Q1+Q2	%Q1+Q2
N-S	1124	12.7	25	30.8	45	31.3
NE-SW	2478	28.1	8	9.9	16	11.1
E-W	3319	37.6	29	35.8	54	37.5
NW-SE	1912	21.6	19	23.5	29	20.1

Q1+Q2+Q3	%Q1+Q2+Q3
53	26.5
24	12
88	44
35	17.5

Table S5

Name	Date	Event location (lat;lon)	Event depth (km)	Moment magnitude	Station code	Station location (lat;lon)
Düzce	11/12/1999	40.81;31.19	10.4	7.3	8101	40.84;31.15
Azores Islands	7/9/1998	38.61;-28.57	10	6.1	HOR	38.53;-28.63
Patti Gulf	4/15/1978	38.27;15.11	22	6.0	MLZ	38.23;15.24
Patti Gulf	4/15/1978	38.27;15.11	22	6.0	PTT1	38.15;14.97
Kyllini	10/16/1988	37.93;20.92	25	5.9	ZAK1	37.79;20.90

Epicentral distance (km)
5.3
10.7
12.5
18.3
15.7

Figure S1

Click here to access/download;Supplemental Material (Main Page, Tables, and Figures);FigS1.png

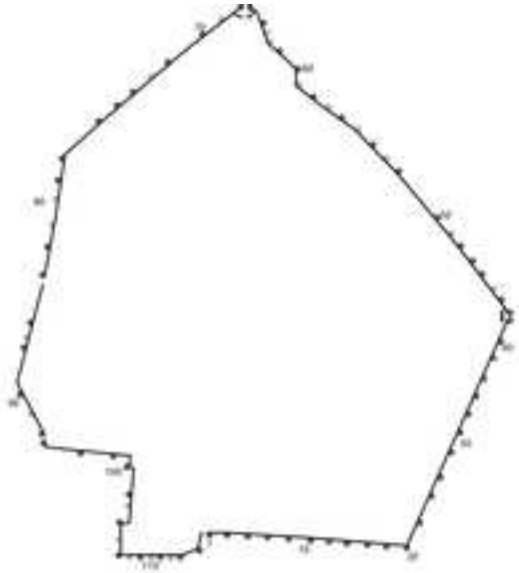

Original 3rd century walls (Claudius Gothicus)

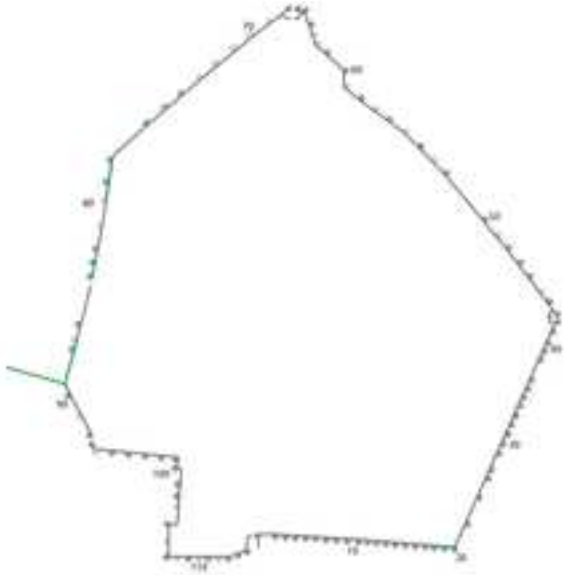

Komnenoi reconstructions (late 11th and 12th c.)

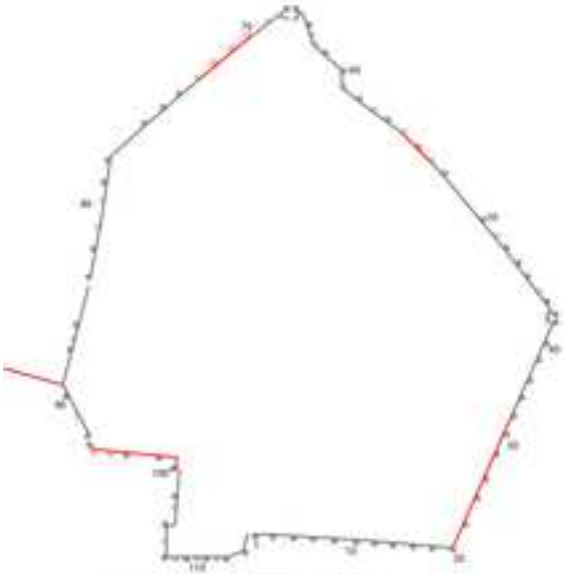

Isaurian reconstructions (c. 730)

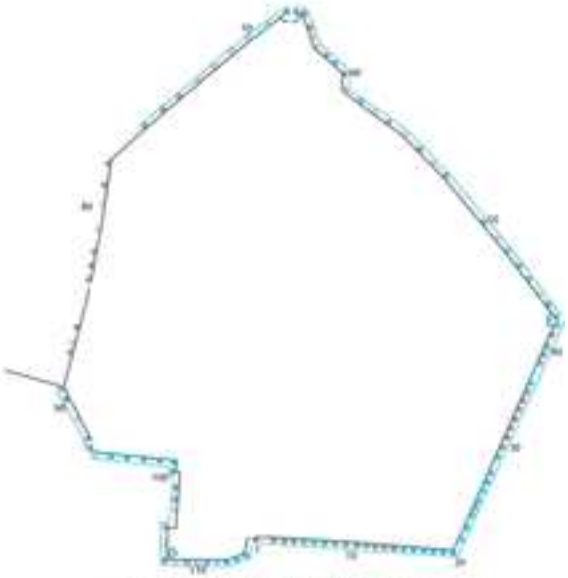

Lascaris reconstructions (1208-1254)

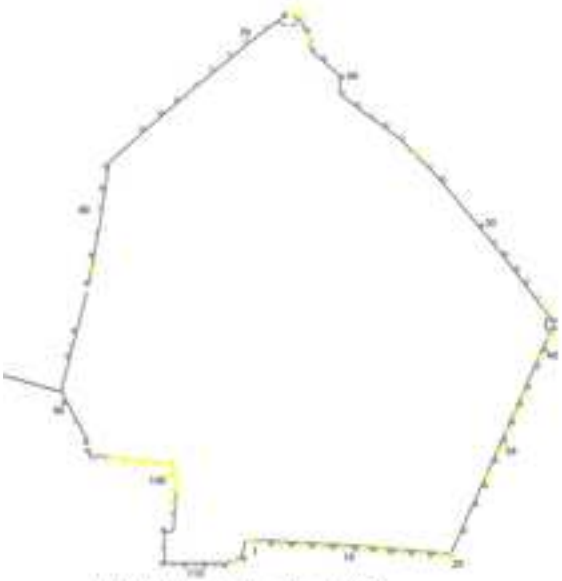

Michael III reconstructions (c. 858)

Palaeologue reconstructions (1254-1331)

Figure S2

Click here to access/download;Supplemental Material (Main Page, Tables, and Figures);FigS2.png